DYNAMIC OPTICAL TWEEZERS GENERATION AND CONTROL USING RING RESONATOR SYSTEM

METHA TASAKORN

A THESIS SUBMITTED IN PARTIAL FULFILLMENT

OF THE REQUIREMENT FOR THE DEGREE OF

DOCTOR OF PHILOSOPHY IN APPLIED PHYSICS

FACULTY OF SCIENCE

KING MONGKUT'S INSTITUTE OF TECHNOLOGY LADKRABANG

2011

KMITL-2011-SC-D-030-031

Thesis Title	Dynamic optical tweezers generation and control using ring resonator system
Student	Mr. Metha Tasakorn
Student ID	52650109
Degree	Doctor of Philosophy
Program	Applied Physics
Year	2011
Thesis Advisor	Assoc. Prof. Dr. Preecha Yupapin

ABSTRACT

This thesis presents the use of nonlinear microring resonator system for optical trapping tool generation, where three cases of studies are proposed. A system is consisted of a microring resonator and an optical add/drop filter, which can be available for optical trapping tool generation, molecule/atom trapping and transportation. Firstly, the X-ray laser sources can be generated and described for medical tool applications, in which the tiny system consists of a series of microring and nanoring resonators, whereas the powerful laser can be amplified to reach the very high power amplification. Secondary, the multitweezers can be generated using a PANDA ring resonator, which is consisted of an add/drop filter and a nanoring resonator. The dark/bright soliton pulses are input into input port and add port respectively. The multiplexing signals of dark/bright soliton pulses are controlled, tuned, and amplified within the system. The optical storage ring are embedded within the add/drop optical filter system, whereas the generated optical signals can be stored and amplified within the design system. The storage signal is controlled and tuned to be an optical probe which can be configured as optical tweezers, where the high filed peak or well can be formed. By using the suitable parameters, we found that tweezers storage time of 1.2 ns is achieved. Therefore, the generated dynamic optical tweezers can be stored and trapped molecule or atom, which can be transmitted and recovered by using the proposed system.

Finally, the dynamic potential well generation and control using light pulse control within an add/drop optical filter. The multiplexing signals of the dark solition with bright or Gaussian pulses are controlled, tuned, and amplified within the system. The optical storage rings are embedded within the add/drop optical filter system, whereas the generated optical signals can be stored and amplified within the design system. In application, the storage signals can be configured to be an optical trapping tool, which is known as an optical tweezer, where the high field peak or well can be formed. The advantages are that the dynamic well can be stored and the array of wells can be generated for multiple wells applications. The different in time of the first two dynamic wells of 1 ns is noted.

หัวข้อวิทยานิพนธ์ การสร้างและควบคุม ที่คีบทางแสงแบบไดนามิก โดยใช้ระบบวงแหวนสั่นพ้อง
นักศึกษา นายเมธา ทัศคร
รหัสประจำตัว 52650109
ปริญญา ปรัชญาดุษฎีบัณฑิต
สาขาวิชา ฟิสิกส์ประยุกต์
พ.ศ. 2554
อาจารย์ที่ปรึกษา รศ.ดร.ปรีชา ยุพาพิน

บทคัดย่อ

งานวิจัยนี้นำเสนอ การสร้างเครื่องมือดักจับทางแสงด้วยระบบวงแหวนสั่นพ้องแบบไม่เป็นเชิงเส้น ระบบประกอบไปด้วยวงแหวนสั่นพ้องระดับไมโครเมตรและตัวกรองสัญญาณแสงแบบเพิ่ม/ลด ที่สามารถใช้สำหรับการสร้างเครื่องมือดักจับทางแสง เพื่อการดักจับและขนส่งอะตอมหรือโมเลกุล ซึ่งได้นำเสนอสามกรณีศึกษาดังนี้ ลำดับแรกนำเสนอการสร้างแหล่งกำเนิดเอกซ์เรย์เลเซอร์ เพื่อประยุกต์ใช้งานด้านการแพทย์ ซึ่งเป็นระบบที่มีขนาดเล็กมากประกอบไปด้วยการอนุกรมกันของวงแหวนสั่นพ้องระดับไมโครและนาโนเมตร ที่สามารถขยายกำลังของแสงเป็นลำแสงเลเซอร์พลังงานสูงได้ ลำดับที่สองนำเสนอการสร้างตัวคีบทางแสงแบบหลายตัวโดยใช้วงแหวนสั่นพ้องแบบ PANDA ซึ่งประกอบไปด้วยตัวกรองสัญญาณแสงแบบเพิ่ม/ลด และวงแหวนสั่นพ้องระดับนาโนเมตร โดยใช้ดาร์คและไบรท์โซลิตอลเป็นสัญญาณให้กับ พอร์ตอินพุต และ พอร์ตแอด ของตัวกรองสัญญาณแสงแบบเพิ่ม/ลด ตามลำดับ ซึ่งจะทำให้เกิดการมัลติเพล็กซ์กันของสัญญาณแสง และสามารถทำการควบคุม ปรับแต่ง และขยายสัญญาณแสงได้ภายในระบบ ในส่วนของวงแหวนที่ใช้กักเก็บพลังงานแสงที่ถูกฝักไว้ในระบบตัวกรองสัญญาณแสงแบบเพิ่ม/ลด สามารถสัญญาณแสงที่เก็บสะสมพลังงานและขยายกำลังได้ภายในระบบที่ออกแบบ ซึ่งสามารถควบคุมและปรับสัญญาณแสงที่เก็บไว้ในระบบให้กลายมาเป็นตัวคีบทางแสงได้ โดยยอดของกำแพงสนามพลังงานแสงจะถูกสร้างขึ้น จากการใช้ค่าพารามิเตอร์ที่เหมาะสมเราพบว่าระบบสามารถเก็บสะสมพลังงานได้นาน 1.2 นาโนวินาที ฉะนั้นการสร้างตัวคีบทางแสงแบบไดนามิกสามารถดักจับโมเลกุลหรืออะตอมและสามารถส่งและรับได้ด้วยระบบที่นำเสนอ อันดับสุดท้ายคือการสร้างบ่อพลังงานศักย์แบบไดนามิกแบบหลายตัว ซึ่งสามารถควบคุมได้จากสัญญาทางแสงที่ถูกส่งผ่านเข้าไปภายตัวกรองสัญญาณแสงแบบเพิ่ม/ลด เกิดการมัลติเพล็กซ์กันของสัญญาณแสงดาร์ทโซลิตอน และ ไวท์โซลิตอน หรือ สัญญาณเกาส์เชียน และสามารถทำการควบคุม ปรับแต่ง และขยายสัญญาณแสงได้ภายในระบบ แหวนเก็บแสงที่ฝังอยู่ภายในตัวกรองสัญญาณแสงแบบเพิ่ม/ลดลง ในขณะที่การสร้างสัญญาณแสงจะถูกเก็บไว้และขยายภายในระบบที่ได้ออกแบบ การนำไปใช้ประยุกต์ใช้งานสัญญาณการจัดเก็บข้อมูลสามารถกำหนดค่าให้เป็นเครื่องมือในการวางกับดักแสงซึ่งเป็นที่รู้จักกันเป็นที่คีบทางแสง โดยที่จุดสูงสุดของสัญญาณแสงจะถูกสร้างขึ้นเป็นขอบเขตหรือเป็นหลุมของพลังงานที่เกิดขึ้น ข้อดีที่ว่ากันแบบไดนามิกสามารถจัดเก็บและอาเรย์ของหลุมก็จะสามารถสร้างสำหรับการใช้งานหลายหลุม ที่แตกต่างกันในช่วงเวลาแรกที่สองหลุมแบบไดนามิกห่างกัน 1 นาโนวินาทีได้ถูกระบุไว้

Acknowledgements

With respect to this research, I am particularly grateful to the Faculty of Industrial and Technology, Rajamamgala University of Technology Isan, Sakon Nakhon Campus and Faculty of Science , King Mongkut's Institute of Technology Ladkrabang for supporting scholarship and providing a study environment that is so conducive to study the doctoral program, and writing this dissertation.

This thesis would not have been possible without the continuous guidance, support and encouragement from my advisor, Associate Professor Dr. Preecha Yupapin. His broad vision, together with his remarkable knowledge of our field of research, has proved to be invaluable in defining my research direction.

I would like to thank my other committee members: Dr.Prathan Boonranasiri, Associate Professor Dr. Thitinai Gaewdang, Associate Professor Dr. Somsak Mitatha and Dr. Nithiroth Pornsuwancharoen for their assistance, helpful comments, and insightful suggestions.

My co-workers at the Nanoscale Science and Engineering Research Alliance (N'SERA) thank them all for their warm friendship and being very supportive.

Finally, I would like to thank my loving parents, who have taught me to achieve my goals, my sister and brother, who have always believed in me. Their unconditional love has been the greatest source of energy to me.

Metha Tasakorn

CONTENTS

CONTENTS (cont.)

CONTENTS (cont.)

LIST OF FIGURES

LIST OF FIGURES (cont.)

Figures **Pages**

LIST OF FIGURES (cont.)

CHAPTER 1

INTRODUCTION

1.1 Introduction

Optical tweezers is a term used to describe the manipulation of microscopic objects using the force of focused laser light. A single laser beam focused to a diffraction limited spot can hold a transparent micro object in the region of highest light intensity due to the three dimensional intensity gradient of the light. The optical tweezers system has become a major tool in biological research over the last forty years, as particles ranging from intracellular structures, such as chromosomes or motor proteins, to whole cells can be readily manipulated.

Laser light was discovered to have the ability to move particles in 1970 by Arthur Ashkin [1], who was based at Bell Telephone Laboratories in New Jersey. Microscopic silica spheres were accelerated along a horizontally directed TEM00 mode laser beam from an argon ion laser by the radiation pressure force of the beam. The particles were drawn into the beam axis by the transverse gradient force of the light and accelerated in the direction of beam propagation due to the scattering force of the light. It was also observed that bubbles (of lower refractive index than the surrounding medium) were repelled away from the centre of the beam as they were simultaneously accelerated in the direction of laser light by the radiation pressure force. Two opposing TEM00 beams were shown to trap spheres of high refractive index. Particles were drawn into the beam axis by the gradient force and accelerated to a stable equilibrium point between the foci of the two counter propagating beams, where the particle was held in position by the opposing radiation pressure forces. The idea of using radiation pressure from laser beams was expanded to include the manipulation of atoms and molecules. It was hypothesized and subsequently shown that absorption and then spontaneous emission of resonant radiation striking the atom could provide a driving force, or pressure, in the direction of light propagation [2].

In 1971 the optical levitation trap for microscopic particles was used for the first time [3]. A focused TEM00 mode laser, directed upwards was shown to support spheres against the downwards pull of gravity using radiation pressure force and to simultaneously hold the particle in the beam centre using the transverse gradient force. Such a levitation trap was used in 1985 to introduce particles into an

alternating light beam trap [4]. Particles were trapped between the foci of the two counter-propagating beams without requiring any gradient force. In 1986 a seminal paper entitled 'Observation of a single-beam gradient force optical trap for dielectric particles' [5] was published. Up until this point, optical traps used radiation pressure force from a laser beam to stably hold particles in the axial direction, either against a counter-propagating beam or against gravity, and the transverse gradient force held the particle in the centre of the Gaussian beam.

In 1986, a single focused laser beam was used to stably trap, in three dimensions, particles ranging in diameter from 25 nm to 10 mm in diameter in water. This trapping was due to both the transverse and the axial gradient force exerted by the focused laser beam – a three dimensional intensity gradient. In the levitation traps the axial stability was dependent on the balance of the scattering force and gravity, but in the single beam gradient force traps the axial gradient force is so large that it dominates the axial stability. This type of single-beam gradient force trap, commonly known as optical tweezers, is now widely used, with applications ranging from investigating the angular momentum of light to measuring intracellular forces. An optical tweezers system is a particularly useful tool for biological studies as the trapping process can be completely non-invasive and sterility of samples can be readily incorporated into existing commercially available microscope system.

The nonlinear effect in optical fibers is due either to changes in the refractive index with optical power or to scattering phenomenal. The power dependence of refractive index is responsible for the Kerr effect. Depending on the shape of the input signal, the Kerr nonlinearity manifests itself by different effect, such as self-phase modulation, cross-phase modulation, Nonlinear behaviors of light traveling in fiber optic are commonly induced by the effects such as Kerr effects[6], four-wave mixing[7], and the external nonlinear pumping power[8]. The nonlinear behaviors occur are named as chaos, bistability and bifurcation [9], the details of such behaviors of light traveling in a micro ring resonator are clearly described by Yupapin et al [10]. However, there are some benefits of the nonlinear behaviors apart from the penalties, one of the behaviors known as chaos has been used to make the benefit in communications in either electronics [11] or optical communications [12]. Unfortunately, the previous investigations are shown in mathematical ways, where the practical applications could not occur. For examples, the chaotic control power input is higher than the standard communication light source using in the system, and the implemented fiber optic devices are not in the fabrication scales.

This means the ability of chaos carriers to synchronize in chaotic communication system is not valid. Recently, Ikeda et al. [13] have reported the successfully fabricated the micro ring resonator with a radius of 10 micron using the optical materials called GaAs-AlGaAs, which is suitable to use in the practical systems. Yupapin [14] have also shown that an Add/drop device could be constructed using a micro ring resonator. The device characteristics that suit to implement in the practical optical tweezers system has seen. To meet the practical applications, the micro ring and Add/drop parameters are needed to make them satisfy the usual fabrication. This thesis presents the design of the system that can be used to generate the dynamic optical tweezers by using the ring resonator system. The nonlinear effect in the ring resonator generated intensity peak that can filter, amplified and multiplex the optics signal within add/drop to generate two nearly intensity peak like the potential well. This signal can be confine the particle such as atom/molecule/DNA. By using the same optical gradient force like the static optical tweezers. The dynamic optical tweezers is not only to trap but also can be move, rotation and transportation via the optical communication system that is the new challenge in this filed. Results obtained have shown that the simulation results with the device parameters having good potentials of practical applications.

1.2 Goal of the Thesis

- Generate X-ray laser source by micro-nanoring resonator using non-linear behavior filter signal, discrete signal and amplified within ring resonator system.
- Generate and control multi dynamic optical tweezers using dark-bright soliton generation control within a nanoring resonator system.
- Atom/molecule/DNA probing and transportation using dynamic optical tweezers via a wavelength router by ring resonator system.

1.3 Scope of the Thesis

Scope of this thesis, we purpose the design parameter of nano-microring resonator waveguide such as: coupling coefficient, ring radii for X-ray laser source and dynamic optical tweezers applications. We show that the control input power can be used to specify the output filtering signal and the power output able to control by radii of ring resonator.

1.4 Organization of the Thesis

This thesis presents a novel simulation and a novel design in application ring resonator. The organization is as follows:

- The current chapter gives an introduction to the subject of the thesis and generalized signal processing in optical tweezer.
- Chapter 2 describes some of theoretical foundation nonlinear optics, optical soliton, optical nano-microring resonator, optical add/drop filter, optical force and optical tweezers.
- Design the ring resonator system by using nonlinear behavior in nano-micro ring resonator and all essential parameters describing the nonlinear characteristics are extracted in chapter 3, 4 and 5.
- Finally, Chapter 6 presents a summary of the results of the thesis and a discussion of future research.

CHAPTER 2

THEORETICAL BACKGROUND

For an understanding of the nonlinear optics in waveguide, it is necessary to consider the theory of electromagnetic wave propagation in dispersive nonlinear media. The objective of this chapter is to obtain discuss fiber characteristics, fiber nonlinearities and basic equation that governs propagation of optical pulses in single mode fibers. We discuss nonlinear in optical fiber ring resonator such as Kerr Effect, Optical chaotic communication, Optical Soliton and Optical Add/Drop Ring Resonator Filter. And also the light-matter interaction is at heart of trapping and the subsequent forces may be understood in a number of way. Perhaps the most straightforward case is to consider an object in the Mie regime; where the particle radius, r, is much larger then the trapping wavelength, λ. When trapping in the Mie regime, one can invoke the use of geometrical ray optics to picture the forces involved. In this chapter, we will discuss different nonlinear processes that affect the performance of semiconductor ring resonators and the optical forces are used to trapping and transport the tiny particle.

2.1 Nonlinear Optics

Nonlinear optics is the study of phenomena that occur as a consequence of the modification optical properties of a material under intense illumination. Typically, only laser light is sufficiently intense to modify the optical properties of a material. Nonlinear optical phenomena are nonlinear in the sense that the induced material polarization is nonlinear in the electric field [15]. The general equation that describes the optical field evolution in a dielectric material is given by

$$\nabla^2\vec{\mathrm{E}} - \frac{1}{c^2}\frac{\partial^2\vec{\mathrm{E}}}{\partial t^2} = -\mu_0\frac{\partial^2\vec{\mathrm{P}}\left(\vec{\mathrm{E}}\right)}{\partial t^2} \tag{2.1}$$

where the polarization $\vec{\mathrm{P}}$ characterizes the medium and it is a function of the electric field. In the case of weak nonlinear behavior of the medium, the polarization can be expressed by a Taylor polynomial as

$$\vec{P} = \underbrace{\varepsilon_0 \vec{E} + \varepsilon_0 \chi^{(1)} : \vec{E}}_{linear\ P_L} + \underbrace{\varepsilon_0 \chi^{(2)} :: \vec{E} \cdot \vec{E} + \varepsilon_0 \chi^{(3)} ::: \vec{E} \cdot \vec{E} \cdot \vec{E} + \ldots}_{nonlinear\ P_{NL}}, \quad (2.2)$$

where dielectric dispersion is ignored. $\chi^{(1)}$ is the linear susceptibility :represents the inner tensor product and the second and the third-order tensor. $\chi^{(2)}$ and $\chi^{(3)}$ are responsible for the second harmonic generation, and the third-order harmonic generation, respectively.

2.1.1 Optical Kerr Effect

Nonlinear effect in optical fibers is due either to change in the refractive index with optical power or to scattering phenomenal. The power dependence of refractive index is responsible for the Kerr effect. Depending on the shape of the input signal, the Kerr nonlinearity manifests itself by different effect, such as self-phase modulation, cross-phase modulation, Nonlinear behaviors of light traveling in fiber optic are commonly induced by the effects such as Kerr effects, four-wave mixing, and the external nonlinear pumping power. The device characteristics that suit to implement in the practical communication system has seen. To meet the practical applications, the micro ring and Add/drop parameters are needed to make them satisfy the usual fabrication. The analogy of chaotic signal generation using fiber ring resonator and the related behaviors are described.

The optical Kerr effect (i.e. nonlinear refractive index) results from the third order nonlinear susceptibility $\chi^{(3)}$, which is a fourth rank tensor.

An optical wave is a real quantity and usually expressed as

$$\vec{E}(t) = \mathrm{Re}\left\{\vec{E} \exp j(\vec{k} \cdot \vec{r} + \omega t)\right\} \quad (2.3)$$

or similarly as

$$\vec{E}(t) = \frac{1}{2}\vec{E} \exp j(\vec{k} \cdot \vec{r} + \omega t) + c.c. \quad (2.4)$$

where c.c. represents the complex conjugate of the preceding term. Thus, an x-polarized optical wave, propagating in the z-direction in an isotropic medium, is represented mathematically as

$$\vec{\mathrm{E}}(t)=\frac{1}{2}\mathrm{E}_x\hat{x}\exp j(kz+\omega t)+c.c. \tag{2.5}$$

The third order polarization (mediated by $\chi^{(3)}$) in a material leads to a nonlinear intensity dependent contribution to its refractive index; i.e., the refractive index of the material changes as the incident intensity on the material changes. The susceptibility tensors in isotropic material can be further simplified as $\chi^{(2)}=0$, due to inversion symmetry; the third order nonlinear susceptibility will only have one contributing term χ_{xxxx} since the light is x-polarized and there are no means for sourcing additional polarization components.

The linear and nonlinear induced polarizations are

$$P_L=\varepsilon_0(1+\chi^{(1)})E, \tag{2.6}$$

$$\begin{aligned}P_{NL}&=P^{(3)}\\&=\varepsilon_0\chi_{xxxx}(\omega;-\omega,\omega,\omega)E^*EE\\&\quad+\varepsilon_0\chi_{xxxx}(\omega;\omega,-\omega,\omega)EE^*E\\&\quad+\varepsilon_0\chi_{xxxx}(\omega;\omega,\omega,-\omega)EEE^*\\&=3\varepsilon_0\chi_{xxxx}|E|^2E\\&=\frac{3}{4}\varepsilon_0\chi_{xxxx}|E_x|^2E\end{aligned} \tag{2.7}$$

respectively. Hence,

$$P=P_L+P_{NL}=\varepsilon_0\left(1+\chi^{(1)}+\frac{3}{4}\varepsilon_0\chi_{xxxx}|E_x|^2\right)E$$

The total dielectric constant is

$$\varepsilon_r^{tot}=\varepsilon_r+\Delta\varepsilon_r$$

where $\varepsilon_r=1+\chi^{(1)}=n_o^2$ and $\Delta\varepsilon=\frac{3}{4}\chi_{xxxx}|E_x|^2$ after comparing with the expression for P. The refractive index is related to the dielectric constant as:

$$n = \sqrt{\varepsilon_r + \Delta\varepsilon_r} \approx \sqrt{\varepsilon_r} + \frac{\Delta\varepsilon_r}{2\sqrt{\varepsilon_r}} = n_0 + \frac{3\chi_{xxxx}}{8n_0}|E_x|^2 \tag{2.8}$$

The intensity dependent refractive index for a nonlinear material is given by

$$n = n_0 + n_2|E|^2 \tag{2.9}$$

Comparing Eq.(2.8) and Eq.(2.9), the nonlinear refractive index is directly determined by the third-order susceptibility as

$$n_2 = \frac{3\chi_{xxxx}}{8n_0} = \frac{3\chi^{(3)}}{8n_0} \tag{2.10}$$

which characterizes the strength of the optical nonlinearity. The intensity I of an optical wave is proportional to $|E|^2$ as $I = \frac{1}{2\eta}|E|^2$ where η is the impedance of the medium. When comparing the optical response in the same medium, $I = |E|^2$ is taken for simplification.

2.1.2 Self-Phase Modulation

The change in refractive index due to the Kerr effect determines a corresponding change in the propagation constant. As a consequence, the phase of a signal propagating through the fiber varies with distance according to the equation:

$$\phi = n_0 k_0 z + \gamma P(t) z \tag{2.11}$$

where $\gamma = n_2 k_0 / A_{eff}$. The first term in Eq. (2.11) represents the linear phase shift due to signal propagation; the second term represents the nonlinear phase shift. When the incident wave is a pulse with a power variation given by $P(t)$, the output pulse is chirped. This phenomenon is called self-phase modulation (SPM), since the power variation within the pulse leads to its own phase modulation. In the leading edge of the pulse, where $dP/dt > 0$, the instantaneous frequency is downshifted from the central frequency, whereas in the trailing edge, where $dP/dt < 0$, the

instantaneous frequency is upshifted. The chirping due to nonlinearity leads to increased spectral broadening.

In the presence of dispersion, the spectral broadening due to SPM determines two situations qualitatively different. In the normal dispersion region (where the wavelength is shorter than the zero dispersion wavelength, λ_{ZD}) the chirping due to dispersion is to downshift the leading edge and to upshift the trailing edge of the pulse, which is a similar effect as that due to SPM. Thus, in this regime the chirping due to dispersion and SPM add. On the other hand, in the anomalous dispersion region, the chirping due to dispersion is opposite to that due to SPM. Consequently, nonlinearity and dispersion induced chirpings can partially or even completely cancel each other. When this cancellation is total, the pulse neither broadens in time nor in its spectrum and such pulse is called a soliton. Much research effort has been devoted to the study of optical solitons and their application in telecommunication systems because they have the peculiar behavior of preserving their shape during propagation [16].

2.1.3 Cross-Phase Modulation

When two or more signals having different carrier frequencies are transmitted simultaneously inside an optical fiber, the nonlinear phase evolution of the signal at frequency ω_i depends also on the power of the other signals. This nonlinear phenomenon is known as cross-phase modulation (XPM) and it is due also to the intensity dependence of the refractive index. The nonlinear phase shift of the signal at ω_i becomes:

$$\phi_i^{NL} = \gamma z \left[P_i + 2 \sum_{i \neq j} P_j \right] \tag{2.12}$$

Where P_j is the power of the signal at ω_j. The first term in the square brackets represents the contribution of SPM, while the second term is the contribution from the XPM. The factor 2 in Eq. (2.12) indicates that XPM is twice as effective as SPM for the same amount of power.

From Eq. (2.12) it can be deduced that XPM is effective only when the interactive signals are superimposed in time. In the presence of finite dispersion, two pulses at different frequencies will move with different velocities and thus the pulses will walk off from each other. Obviously, larger dispersion will reduce the walk off length and hence the XPM effects.

Due to XPM, the phase of each channel in a WDM system is affected by both the average power and the bit pattern of all other channels. Fiber dispersion converts phase variations into amplitude fluctuations that affect the signal-to-noise ratio (SNR) and introduce jitter. In these circumstances, an understanding of the interplay between XPM and GVD is very important for WDM systems [17].

2.1.4 Four Wave Mixing

When the signal at difference frequencies propagates through the medium, besides Cross-Phase Modulation (XPM), another important effect occurs: four-wave mixing (FWM) [18].

Four-wave mixing is a nonlinear effect arising from a third-order optical nonlinearity, as is described with a $\chi^{(3)}$ coefficient. It can occur if at least two different frequency components propagate together in a nonlinear medium such as an optical fiber. Assuming just two input frequency components ω_1 and ω_2 (with $\omega_2 > \omega_1$), a refractive index modulation at the difference frequency occurs, which creates to additional frequency components (Fig 2.1). In effect, two new frequency components are generated: $\omega_3 = \omega_1 - (\omega_2 - \omega_1) = 2\omega_1 - \omega_2$ and $\omega_4 = \omega_2 + (\omega_2 - \omega_1) = 2\omega_2 - \omega_1$

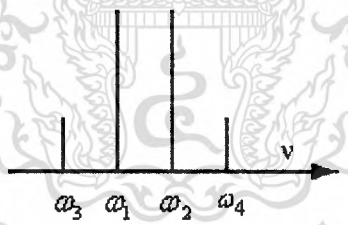

Figure 2.1: Generation of new frequency components via four-wave-mixing

Four-wave mixing (FWM) is a parametric interaction among waves satisfying a given phase relationship called phase matching. Different phenomena may be originated by FWM process depending on the relation among interaction frequencies. If three optical fields with carrier frequencies ω_i (i = 1, 2, 3) co propagates inside the medium simultaneously, it appears that the third-order polarization vector has several components: three components have the frequencies of the input fields, the others have an angular frequency ω_4 given by

$$\omega_4 = \omega_1 \pm \omega_2 \pm \omega_3 \quad (2.13)$$

If no field is present in the medium at the frequency ω_4, a new field component is created at this frequency. If a field at the frequency ω_4 is already present in the medium, it will be affected by the nonlinear interaction between the fields at ω_i, which causes crosstalk in multi-channel communication systems.

The phase-mismatch among all for waves is given by

$$\Delta\beta = \beta(\omega_1) + \beta(\omega_2) - \beta(\omega_3) - \beta(\omega_4) \tag{2.14}$$

where $\beta(\omega)$ is the propagation constant for an optical field with frequency ω. Assuming that the frequencies to be closely and equally spaced (i.e., $\omega_1 = \omega_2 - \Delta\omega$, $\omega_3 = \omega_2 - 2\Delta\omega$, $\omega_1 = \omega_2 - \Delta\omega$) and making a Taylor series expansion of all βs about the frequency ω_2, we get

$$\Delta\beta = 2\beta_2(\Delta\omega)^2 \tag{2.15}$$

where $\beta_2 = \partial^2\beta / \partial\omega^2$ is the group velocity dispersion (GVD). When $\beta_2 = 0$ we a perfect shave-phase matching and thus an efficient FWM. This situation is desirable for applications such as all-optical signal processing, wavelength conversion, pulse compression, etc. FWM in optical materials can also be used for generating spectrally inverted signal through the process of optical phase conjugation (OPC), which is useful for dispersion compensation. However, in WDM systems FWM causes a transfer of power from each channel to its neighbors. Such a power transfer not only results in the power loss for the channel but also induces inters channel crosstalk that degrades the system performance severely. This problem can be minimized using the technique of dispersion management, in which the dispersion is kept locally high even though it is low on average.

2.2 Ring Resonators

A ring resonator is simply a waveguide shaped into a ring structure as shown in Fig. 2.2. When an input electric field, E_i, is coupled to the ring waveguide through an external bus waveguide, a positive feedback is induced and the field inside the ring resonator E_r, starts to build up. Coupling between the straight and the ring waveguide is achieved through the evanescent wave. Therefore, the gap and coupling length between them determine how much power is coupled from the straight waveguide to the ring waveguide and vise versa. In such configuration, only certain

wavelengths will be allowed to resonate inside the ring waveguide, thus frequency selectivity is obtained. A resonant mode will have a wavelength that satisfies.

$$m\lambda_m = nL, \quad \text{m = integer} \tag{2.16}$$

Here, m is the longitudinal mode number, λ_m is the resonant mode wavelength, n is the refractive index of the guiding material, and L is the circumference of the ring resonator.

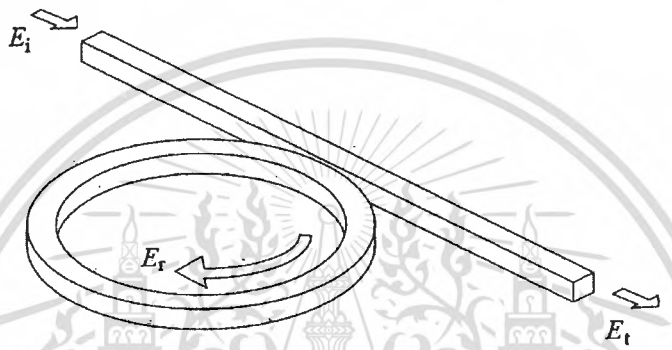

Figure 2.2: Schematic diagram for a ring resonator coupled to a single waveguide.

A ring resonator device is promising candidates for wavelength filtering, multiplexing/demultiplexing, conversion and network routing application. Two typical settings of ring resonator are shown in Fig. 2.3. A ring or a disk shaped dielectric cavity is placed between two parallel dielectric straight waveguides. In real life (3-D) devices, the straight waveguides can be positioned either in the same plane (Fig. 2.3(a): horizontal coupling scheme) or below (Fig. 2.3(b): vertical coupling scheme) the cavity plane. These two straight waveguides form four ports for the external connections, the two input ports named "In-port" And "Add-port", and the two output ports named "Through-port" and "Drop-port". To understand the functioning of the ring resonator, for the sake of simplicity, let's consider only unidirectional fields (clockwise propagating), where only the In-port is illuminated, while there is no incoming signal at the Add-port.

Conventionally, the functioning of ring resonator is described by the interaction of harmonic optical waves propagating along the straight waveguide and the cavity, and the interferometric resonances of the waves inside the cavity. A single frequency optical wave is launched at the In port of the resonator. As this signal propagates along the upper straight waveguide, that connects the In-port and Through-port, part of it is evanescently coupled to the

cavity. While propagating along the cavity, part of this signal is coupled to the lower straight waveguide and appears at the Drop-port. The remaining part of the signal propagates along the cavity, and interferes with the newly in-coupled signal in the upper interaction region. Depending upon the specific configuration, these two fields undergo constructive or destructive interference.

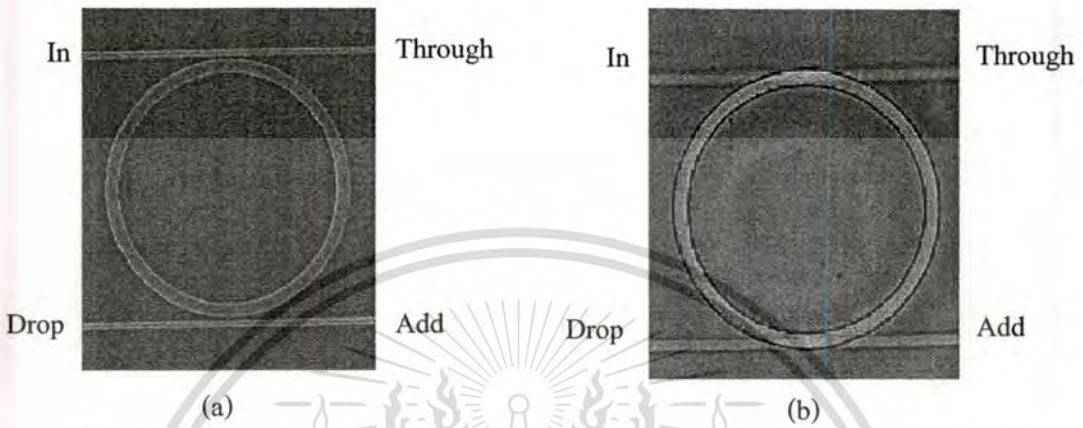

Figure 2.3: Scanning electron microscope pictures of horizontally coupled (a) and vertically coupled (b) real life ring resonator.

If the cavity field is out of phase with the newly entering field, then destructive interference takes place inside the cavity and as a result, there is only a small amount of power inside the cavity. Under so-called off resonance conditions, as shown in Fig. 2.4(a), most of the input power is directly transmitted to the Through-port, and there is comparably low power at the Drop-port.

On the other hand, if the field inside the cavity is in phase with the newly in-coupled signal, then due to constructive interference, energy builds up inside the cavity. This field gets coupled to the Drop-port waveguide. Under so-called resonance conditions, there is a significant power observed at the Drop-port, while less power appears at the Through-port. This situation is shown in Fig. 2.4(b).

A typical spectral response of a ring resonator device is shown in Fig. 2.4(c). Resonance appears as dips in the Through-port power curve and peaks in the Drop-port power curve. In other words, the wavelength for which ring resonator is on resonance, will be "dropped" at the Drop port. Also, for a symmetrical device, if a new signal that corresponds to a resonance wavelength is launched at the Add-port, it will get .added. to the off resonance signal launched at the input port, and appears at the throughput port. Therefore the arrangement shown in Fig. 2.3 can be used as an add/drop filter.

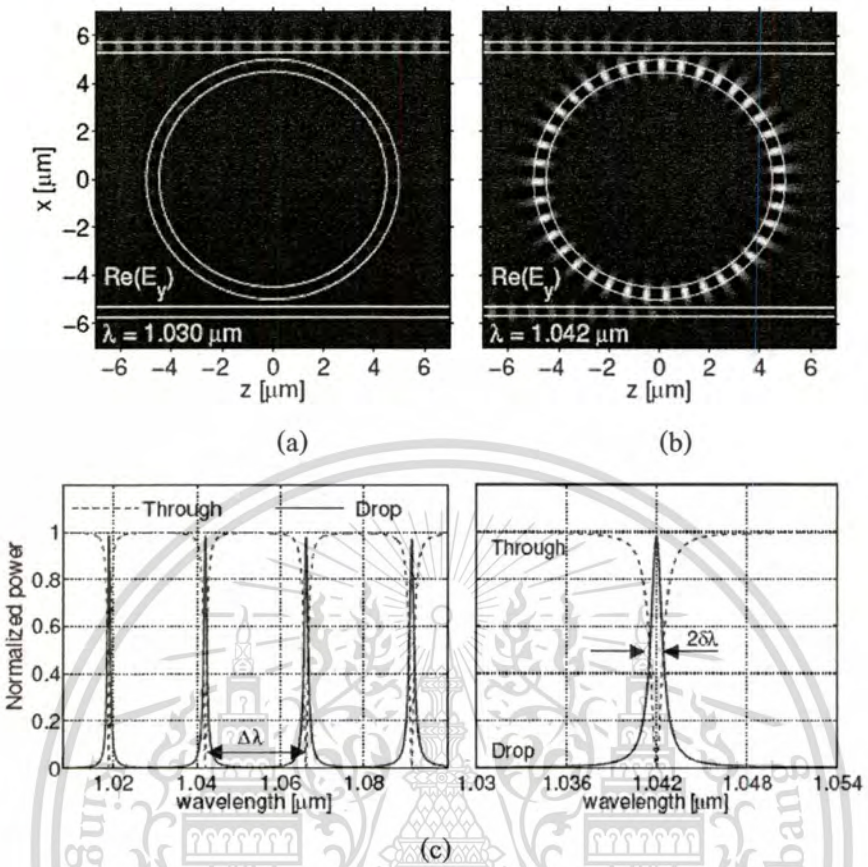

Figure 2.4: Simulated response off-resonance state (a) and resonance state (b) of a ring resonator. Also shown is the wavelength dependent response of the ring resonator (c).

2.2.1 Single Coupler Ring Resonator Filter (SCRR)

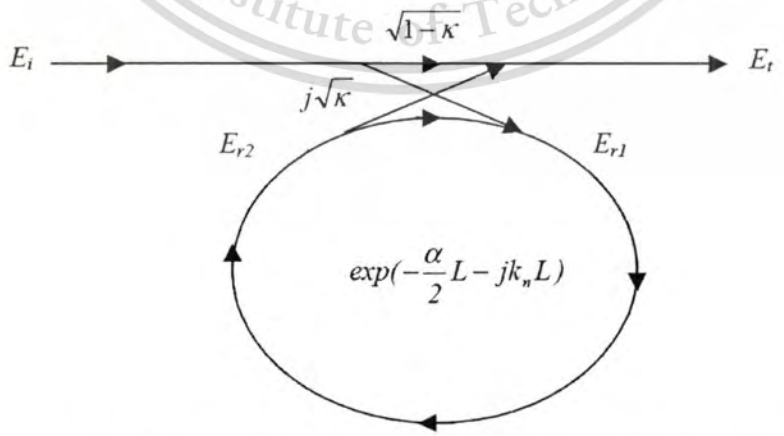

Figure 2.5: Schematic diagram for a ring resonator coupled to a single waveguide

The transfer function of this configuration is derived using Z-transform analysis. The circumference of the ring is L ($L = 2\pi R$, the radius is R), the coupling coefficient of the coupler is κ. The Z-transform parameter is represented by $z^{-1} = \exp^{-jk_n L}$ where $k_n = \frac{2\pi}{\lambda} n_{eff}$ is the propagation constant and n_{eff} is the effective index of the waveguide. The one round trip loss is $a = \exp^{-\alpha L/2}$, α is the intensity attenuation coefficient inside the waveguide [unit $length^{-1}$]. The transmitted or throughput field at the output of the straight waveguide, E_t and inserted electric field, E_i relations can be derived as followed:

$$E_t = (1-\gamma)^{1/2} \times \left[E_i \cdot \sqrt{1-\kappa} + j \cdot E_{r2}\sqrt{\kappa}\right]. \tag{2.17}$$

$$E_{r1} = (1-\gamma)^{1/2} \times \left[j \cdot E_i \cdot \sqrt{\kappa} + E_{r2} \cdot \sqrt{1-\kappa}\right]. \tag{2.18}$$

$$E_{r2} = E_{r1} \cdot a\, z^{-1}. \tag{2.19}$$

Using these equations, E_t / E_i can be calculated:

$$\frac{E_t}{E_i} = (1-\gamma)^{1/2} \times \left[\frac{\sqrt{1-\kappa} - (1-\gamma)^{1/2} \cdot a z^{-1}}{1 - (1-\gamma)^{1/2} \cdot \sqrt{1-\kappa} \cdot a z^{-1}}\right]. \tag{2.20}$$

The transfer function in Eq. (2.20) indicates that a ring resonator is very similar to a Fabry-Perot cavity. In the particular case shown in Fig. 2.5, the corresponding Fabry-Perot cavity would have an input mirror with a field reflectivity and a fully reflecting output mirror. However, the field propagating inside the ring cavity is a traveling wave in contrast to the Fabry-Perot cavity which resonates a standing wave.

In the following, new parameter will be used for simplification:

$$\begin{aligned} D &= (1-\gamma)^{1/2} \\ x &= D \cdot \exp^{-\alpha L/2} \\ y &= \sqrt{1-\kappa} \\ \phi &= k_n \cdot L \end{aligned} \tag{2.21}$$

The intensity relation for the output port is given by:

$$T = \frac{I_t}{I_i}(\phi) = \left|\frac{E_t}{E_i}\right|^2 = D^2 \cdot \left[1 - \frac{(1-x^2)\cdot(1-y^2)}{(1-x\cdot y)^2 + 4\cdot x\cdot y\cdot sin^2\left(\frac{\phi}{2}\right)}\right]. \quad (2.22)$$

2.2.2 Double Coupler Ring Resonator Filter (DCRR)

Consider the architectures of double coupler ring resonator which sometime called add/drop filters as illustrated in Fig. 2.6, which are constructed by 2×2 optical couplers.

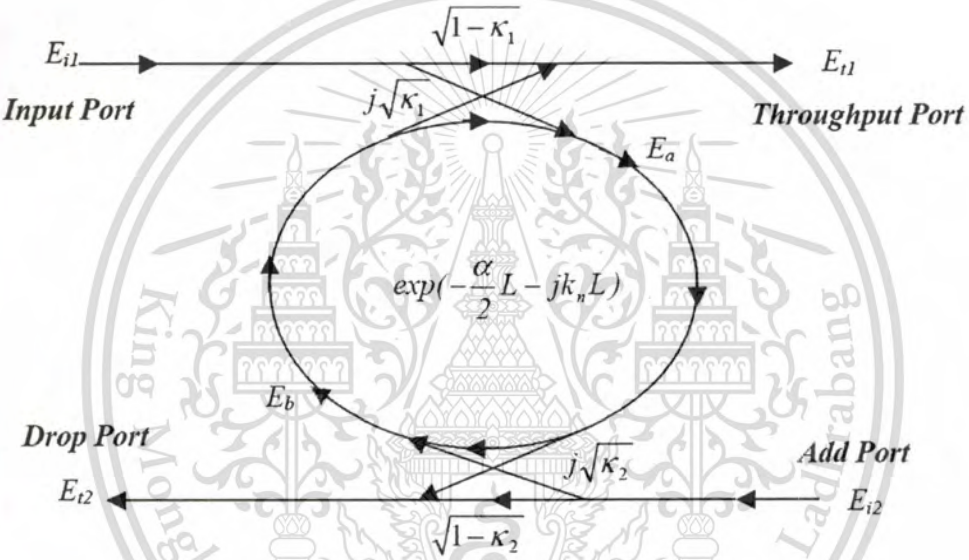

Figure 2.6: The single ring resonator with two adjacent waveguides

For simplification, the calculation of the intensity relation does not take into account coupling losses ($D^2 = 1$).

$$E_a = E_{i1}\, j\sqrt{\kappa_1} + E_b\sqrt{1-\kappa_1}\, e^{-\frac{\alpha}{2}\frac{L}{2} - jkn\frac{L}{2}} \quad (2.23)$$

$$E_b = E_a\sqrt{1-\kappa_2}\, e^{-\frac{\alpha}{2}\frac{L}{2} - jkn\frac{L}{2}} \quad (2.24)$$

$$E_a = \frac{E_{i1}\, j\sqrt{\kappa_1}}{1-\sqrt{1-\kappa_1}\sqrt{1-\kappa_2}\, e^{-\frac{\alpha}{2}L - jknL}} \quad (2.25)$$

$$E_b = \frac{E_{i1}\, j\sqrt{\kappa_1}}{1-\sqrt{1-\kappa_1}\sqrt{1-\kappa_2}\, e^{-\frac{\alpha}{2}L-jknL}} \cdot \sqrt{1-\kappa_2}\, e^{-\frac{\alpha L}{2\,2}-jkn\frac{L}{2}} \tag{2.26}$$

$$E_{t1} = E_b\, j\sqrt{\kappa_1}\; e^{-\frac{\alpha L}{2\,2}-jkn\frac{L}{2}} + E_{i1}\sqrt{1-\kappa_1} \tag{2.27}$$

$$E_{t2} = E_a\, j\sqrt{\kappa_2}\; e^{-\frac{\alpha L}{2\,2}-jkn\frac{L}{2}} \qquad at \;\; E_{i2} = 0 \tag{2.28}$$

Where E_{i1} is the input field, E_{t1} is the throughput field, E_{t2} is the dropped field, E_{t1}, E_a and E_b are the fields in the ring, κ_1 is the field coupling coefficient between the input bus and the ring, κ_2 is the field coupling coefficient between the ring and the input bus, L is the circumference of the ring,

By using the upper equations, the transfer function for throughput port and drop port in Fig. 2.6 can thus be expressed as

Throughput port:

$$\frac{E_{t1}}{E_{i1}} = \frac{-\kappa_1\sqrt{1-\kappa_2}\, e^{-\frac{\alpha}{2}L-jknL} + \sqrt{1-\kappa_1} - (1-\kappa_1)\sqrt{1-\kappa_2}\, e^{-\frac{\alpha}{2}L-jknL}}{1-\sqrt{1-\kappa_1}\sqrt{1-\kappa_2}\, e^{-\frac{\alpha}{2}L-jknL}} \tag{2.29}$$

$$\frac{E_{t1}}{E_{i1}} = \frac{-\sqrt{1-\kappa_2}\, e^{-\frac{\alpha}{2}L-jknL} + \sqrt{1-\kappa_1}}{1-\sqrt{1-\kappa_1}\sqrt{1-\kappa_2}\, e^{-\frac{\alpha}{2}L-jknL}} \tag{2.30}$$

Drop port:

$$\frac{E_{t2}}{E_{i1}} = \frac{-\sqrt{\kappa_1\,\kappa_2}\; e^{-\frac{\alpha L}{2\,2}-jkn\frac{L}{2}}}{1-\sqrt{1-\kappa_1}\sqrt{1-\kappa_2}\, e^{-\frac{\alpha}{2}L-jknL}} \tag{2.31}$$

The intensity relations for the throughput and drop port can be obtained by normalizing the transfer functions in Eqs. (2.32) and (2.33) which are given by

$$\frac{I_{t1}}{I_{i1}} = \left|\frac{E_{t1}}{E_{i1}}\right|^2 = \frac{1-\kappa_1-2\sqrt{1-\kappa_1}\sqrt{1-\kappa_2}\,e^{-\frac{\alpha}{2}L}\cos(knL)+(1-\kappa_2)e^{-\alpha L}}{1+(1-\kappa_1)(1-\kappa_2)e^{-\alpha L}-2\sqrt{1-\kappa_1}\sqrt{1-\kappa_2}\,e^{-\frac{\alpha}{2}L}\cos(knL)} \tag{2.32}$$

$$\frac{I_{t2}}{I_{i1}} = \left|\frac{E_{t2}}{E_{i1}}\right|^2 = \frac{\kappa_1\kappa_2\,e^{-\frac{\alpha}{2}L}}{1+(1-\kappa_1)(1-\kappa_2)e^{-\alpha L}-2\sqrt{1-\kappa_1}\sqrt{1-\kappa_2}\,e^{-\frac{\alpha}{2}L}\cos(knL)} \tag{2.33}$$

2.3 Optical Tweezers and Optical Trapping

2.3.1 Introduction

Optical tweezers find nowadays application in a wide range of disciplines, from physics to biology. The first observations of radiation pressure, i.e. the force exerted by electromagnetic radiation on matter, date back to 1609 when German astronomer Johannes Kepler noticed that the tails of comets always point away from the Sun, being blown by what he believed to be a kind of solar breeze. The fact that electromagnetic radiation exerts a pressure upon a surface exposed to it was deduced theoretically by James Clerck Maxwell in 1871, and proven experimentally by Lebedev in 1900 and by Nichols and Hull in 1901. Experiments on radiation pressure using lasers were performed by Arthur Ashkin in the early 70s at AT&T Bell Telephone Laboratories [1, 3]. He observed that objects of high refractive index were drawn towards the center of an unfocused laser beam, and pushed in the direction of propagation. Three-dimensional trapping of objects could be performed by using two counter-propagating beams. These observations led to the invention in 1986 of the so-called single beam gradient force optical trap [19]. In their seminal paper, Ashkin and co-workers demonstrated that a single, tightly focused laser beam could be used to trap microscopic dielectric particles in three dimensions. In the following year, Ashkin also pioneered the biological application of optical tweezers by trapping Tobacco mosaic virus and single Escherichia coli bacteria [2] and by manipulating particles within the cytoplasm of cells [5].

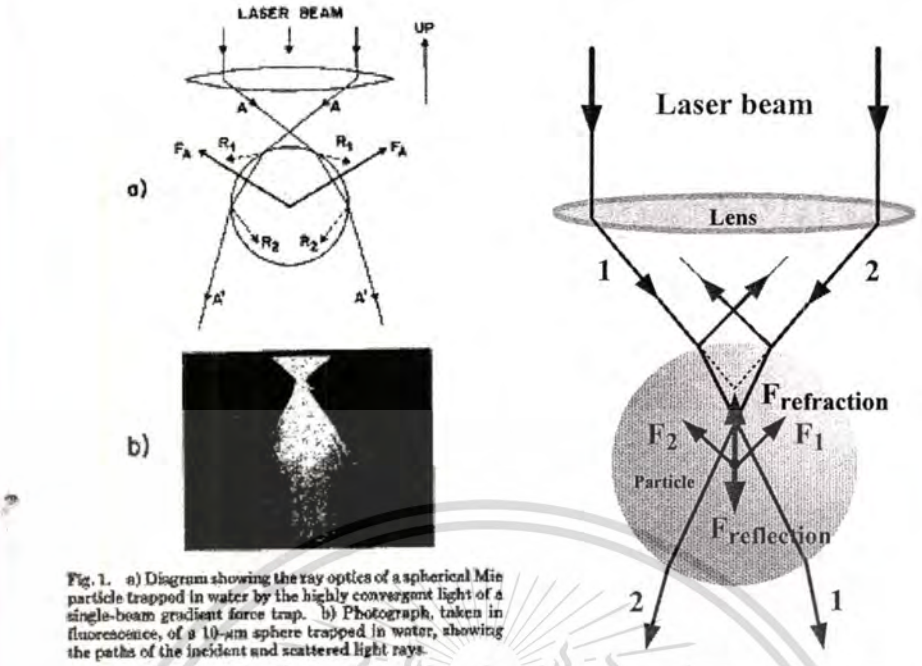

Fig. 1. a) Diagram showing the ray optics of a spherical Mie particle trapped in water by the highly convergent light of a single-beam gradient force trap. b) Photograph, taken in fluorescence, of a 10-μm sphere trapped in water, showing the paths of the incident and scattered light rays.

Figure 2.7: Figure from the 1986 seminal paper by Ashkin and co-workers, demonstrating single-beam gradient force optical trapping. From [5].

The past four decades have seen optical tweezers become a commonplace tool for applications as diverse as cooling atoms [20] and confining Bose-Einstein condensates [21], manipulating and sorting microscopic particles [22], and probing cellular [23] and biomolecular properties [24]. The original setup, based on a laser beam focused through a high-numerical aperture microscope objective, has been improved to accommodate different experimental requirements. Optical tweezers can trap objects as small as 5 nm [25] and can exert forces exceeding 100 pN [26] with sub-pN resolution. This is the ideal range for exerting forces on biological and macromolecular systems and for measuring their responses. As a consequence, optical tweezers have also become a well-established technique for single-molecule studies.

2.3.2 The mechanism of optical trapping

Although the theory behind optical tweezers is still being developed, the basic principles are straightforward for objects either much smaller than the wavelength of light or much larger. Small objects develop an electric dipole moment in response to the light's electric field, which is drawn up intensity gradients in the electric field, toward the focus. Such optical gradient force competes with the scattering component of radiation pressure, which pushes particles down the optical axis. Stable trapping thus requires the axial gradient force to dominate, and is achieved when

the beam diverges rapidly enough away from the focal point. For this reason, optical tweezers are usually constructed around microscope objective lenses, whose high numerical apertures and well corrected aberrations focus light as tightly as possible. Larger objects act as lenses, refracting the rays of light and redirecting the momentum of photons. Intense optical fields can also induce forces between dielectric microparticles, leading to the phenomenon known as optical binding [27]. In order to understand the forces acting within optical tweezers, it is useful to adopt this latter approach, which through ray-optics makes the working principle immediately apparent. Since a light beam carries a linear momentum of h/λ per photon, the refraction of light by a transparent particle results in a change in photon momentum, and a corresponding reaction force acting on the object. In Figure 2.8 one can see that the force arising from refraction of a light ray acts to move the object towards the center of the beam. Furthermore, when the beam is tightly focused a force acts to lift the object towards the focus, thus creating a three-dimensional confinement. The ray-optics approximation holds when the wavelength of the laser is considerably smaller than the size of the object, and a model for evaluating the trapping force based on this approximation will be presented in further.

2.3.3 Multiple tweezers

Optical tweezers can be configured using multiple beams to simultaneously trap more than one particle. Multiple beams of light passing simultaneously through

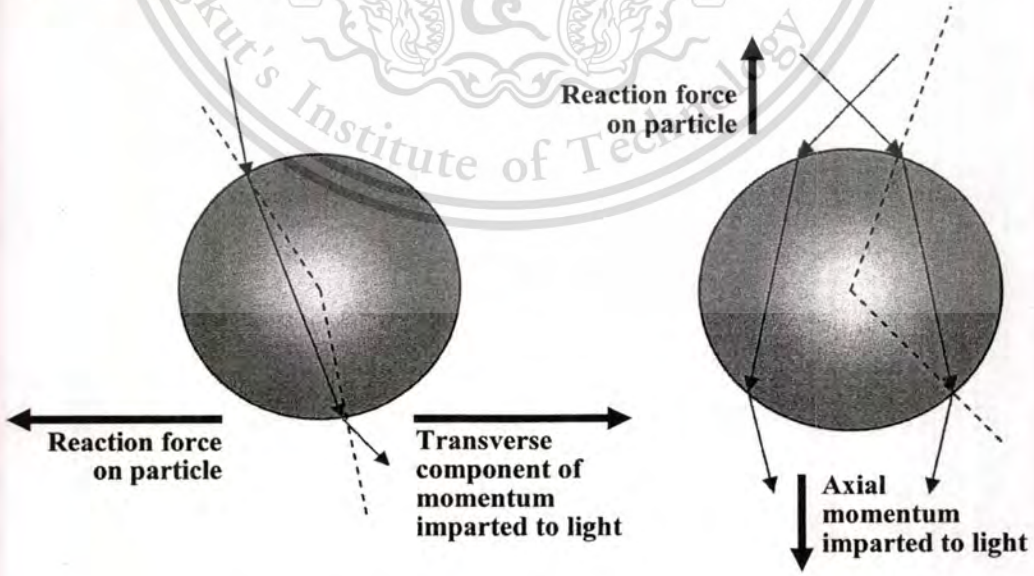

Figure 2.8: Origin of the lateral and axial trapping force in optical tweezers within a ray optics approach.

the objective's entrance pupil focus indeed to multiple optical tweezers, the location of which is determined by the associated beam's angle of incidence and degree of collimation as it enters the objective. Multiple traps have been implemented by the rapid scanning of a single beam between two or more trap positions [28], or by splitting the incident beam to produce multiple light paths which are later recombined before entering the microscope. Their interference at the input pupil gives an amplitude and a phase pattern that characterize the downstream trapping pattern. Imposing the same modulations on a single incident beam at the input pupil would yield the same pattern of traps. Such wavefront modification can be performed by a computer-generated diffractive optical element (DOE), or hologram [22]. A computer-addressed spatial light modulator (SLM) can be used to project sequences of DOEs almost in real time [29-33] so that by slightly displacing the traps from one pattern to the next the particles are transferred along arbitrary three-dimensional (3D) trajectories. A different technique for generating multiple traps with an SLM is based on the generalized phase contrast (GPC) technique, where a pattern of phase modulations on the SLM is directly converted into the corresponding intensity modulation in the focal plane of the objective lens [34] and thus creates arbitrary planar trapping patterns. The conversion involves an annular phase plate similar to that used in the phase-contrast imaging method. The GPC approach avoids the need to calculate holograms and thus is extremely efficient. However, the spatial resolution of existing SLMs currently limits this technique to creating lateral traps rather than 3D optical tweezers.

2.3.4 Forces involved in optical tweezers

2.3.4.1 Mie and Rayleigh regimes

Understanding of the forces involved in optical tweezers can be elucidated by taking two approaches, one based on ray optics for particles in the Mie regime (where the diameter is large compared to wavelength, λ) and the other based on the electric field associated with the light for Rayleigh particles (diameter smaller than λ). Particles in the Rayleigh and Mie regimes compared to λ can be seen in figure 2.9.

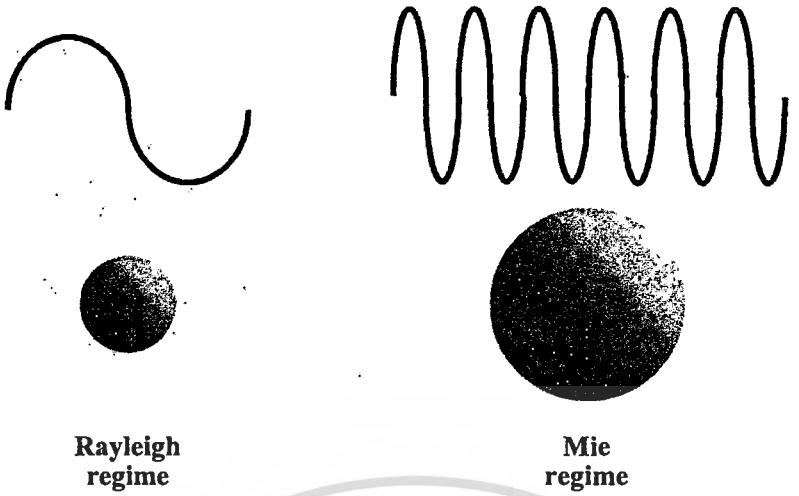

Figure 2.9: The Rayleigh and Mie regimes. In the Rayleigh regime the particle is much smaller than the wavelength of light and in the Mie regime the particle is larger than the wavelength of light.

2.3.4.2 Interaction between light and Mie particles

A ray optics approach is used to calculate forces acting on a particle with a diameter larger than the wavelength of laser light (the Mie regime). The effect of a laser beam on a transparent sphere can be modeled using a bundle of rays, in a similar manner to ray-tracing packages that are used for lens design, with each ray weighted according to its intensity. A photon of wavelength λ has a momentum $p = h/\lambda$ (or $\hbar k$) where h is Plank's constant, $\hbar$ is $h/2\pi$, and k is wave number. If an object causes light to change direction, for instance on reflection or refraction, the change in momentum of the light will exert an equal but opposite change of momentum on the object. This force exerted on an object is not large enough to move macroscopic objects however, the forces involved in the transfer of momentum from focused laser light to microscopic objects are of the order of picoNewtons and can move micron sized particles. Within the Mie regime, if a transparent microscopic particle is situated within a gradient of light, the refraction of rays of differing intensity (due to the gradient) through the particle results in a change in total momentum of the exiting light beam, and hence a corresponding reaction force on the particle, which draws the particle into the region of highest light intensity of the beam (Figure 2.10). An equilibrium position is reached and the particle is held in the centre of the beam as the rays of light passing through and exiting the particle are balanced with no overall change in momentum of the beam. This trapping force is due to the transverse gradient force which is a result of the Gaussian intensity distribution of the laser

mode, however an axial gradient is also required in order to lift the particle and manipulate it in three dimensions. Axial trapping in the z (vertical) direction, which results in a three dimensional trap or so-called optical tweezers, is a result of the axial gradient force which is created by the tight focusing of the laser beam. Off-axis rays come in at an angle towards the particle and gain momentum in the direction of beam propagation. This change in momentum leads to a force which pushes the sphere upwards against the direction of beam propagation towards the focal region of the beam resulting in a trapping force in the z-direction, and thus a three dimensional, optical trap. The equilibrium position is reached when the scattering force and gravity (which both act to push the sphere downwards) is balanced by the axial gradient force (which pushes the sphere upwards).

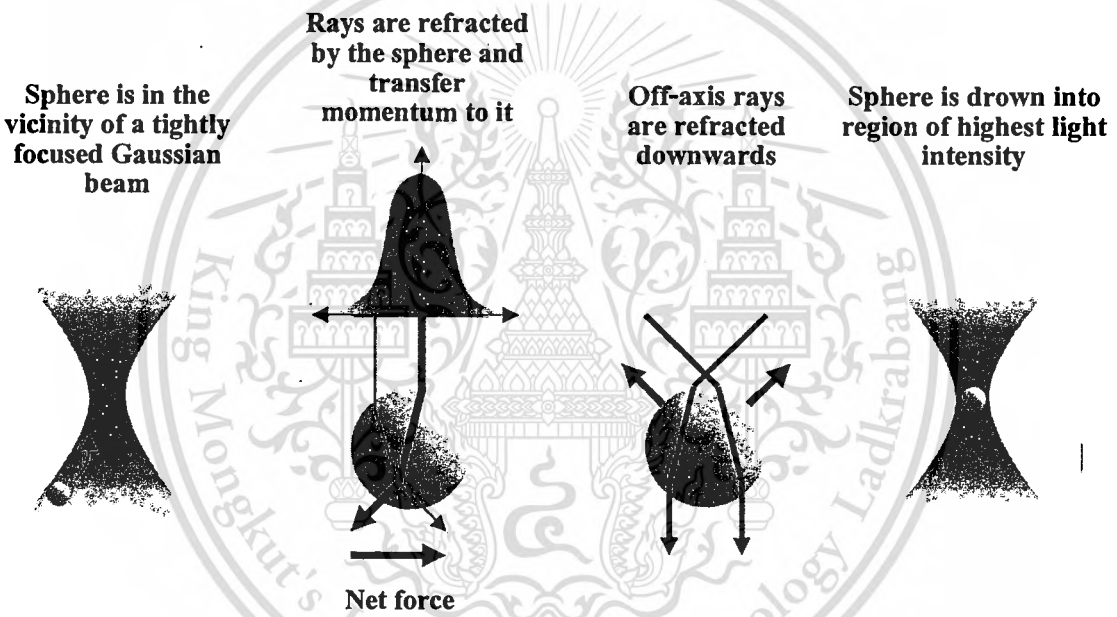

Figure 2.10: Trapping forces. The rays of a Gaussian beam are refracted as they pass through a particle of higher refractive index than the surrounding medium. The intensity gradient of the beam leads to the particle being drawn into the region of highest light intensity. Off axis rays contribute to axial trapping by being refracted in the direction of beam propagation. A force is exerted on the particle of equal but opposite size to the change of momentum of the light.

On axis rays are detrimental to the axial trapping ability of the tweezers when the laser beam is directed into the sample from above. The reflected (or backscattered) component of the on-axis rays gives rise to radiation pressure and exerts a force on the particle in the direction of beam propagation. This results in the particle being pushed downwards, away from the beam focus.

2.3.4.3 Trapping Rayleigh particles

For particles in the Rayleigh regime the ray optics approach is not sufficient to calculate forces as only a fraction of the wave has an effect on the particle. It is better to consider the force in terms of the electric field in the region of the trapped particle. When a polarisable particle is placed in an electric field it will develop an electric dipole moment in response to the light's electric field and is drawn up intensity gradients in the electric field towards the focus (if the polarisability is +ve, i.e. relative refractive index > 1). The energy of the system will be at a minimum when the particle moves to wherever the field is highest – which is at the focus. Optically trapped particles discussed in this work (chromosomes, dielectric silica spheres etc.) lie primarily in the Mie regime, although some DNA particles and 1 mm diameter spheres have sizes comparable to the wavelength of the IR trapping light and are intermediate between the Mie and Rayleigh regime.

2.3.4.4 Trap efficiency

The force on a spherical particle of radius r can be calculated using the viscous drag exerted by moving the particle at a velocity v through a fluid of viscosity η (Stoke's law) when the particle is more than a few diameters away from the sample cell walls and is given by:

$$F_{stokes} = 6\pi\eta r v \tag{2.34}$$

This is the maximum force that the optical trap can exert at the specified laser power and will typically be of the order of picoNewtons [35]. The critical velocity of the trapped particle scales linearly with the laser power in the optical trap (as shown in eq. 2.35). The trapping efficiency of any optical tweezers configuration is usually described in terms of a dimensionless parameter Q, the fraction of momentum transferred to the trapping force from the trapping laser beam, which is related to the force on the sphere, F_{stokes}, the power of the laser, P, and the refractive index of the surrounding medium, n, through the equation

$$F_{stokes} = \frac{nQP}{c} \tag{2.35}$$

Possible values of Q range between 0 and 1. A Q value of 1 corresponds to all of the light beam's momentum being transferred to the particle. Optical tweezers configurations can be assessed

experimentally to determine the Q values for trap efficiency in the lateral and axial directions. For optical forces acting on small dielectric particles Q values tend to be in the range 0.03 to 0.1 [36]. Within conventional optical tweezers Q_{axial} is usually an order of magnitude smaller than $Q_{lateral}$ [37].

2.3.4.5 Trap stiffness

The displacement of the trapped object from the centre of the trap, under an applied viscous fluid force can be monitored using a position sensitive detector. This determines the spring (elastic) constant, in other words the stiffness of the optical trap. Optical tweezers stiffness can also be calculated from analysis of the thermal motion of the trapped object [35, 38]. Trap stiffness tends to be in the range 0.001 to 1 pN nm^{-1} [36] depending on the application. Optical tweezers can also be placed under feedback control so that any particle movement out of equilibrium position can be immediately corrected by repositioning of the trap itself, so that the particle remains stationary within the trap. It is necessary to measure optical trap stiffness before investigating very low forces such as those in biological processes which are discussed later in this chapter. Biologists are mainly concerned with measuring trap stiffness so that molecular forces can be measured, whereas physicists are more interested in the Q value of an optical trap (efficiency), which can be calculated both theoretically and experimentally. In chapter four we calculate the Q value of an optical trap experimentally by measuring the maximum velocity that a trapped particle can be dragged through a viscous medium.

2.4 Summary

This chapter consists of interest for this thesis. That is nonlinearity behavior in a fiber ring resonator, a micro ring resonator and add/drop multiplexer in micro ring resonator, which appeared to the penalty and optical trapping use the forces of light to trapping atom/molecule of transparence object such as cell biology. In addition to presenting theoretical background the nonlinear equation and simple overview of nonlinear phenomenal and the basic theory of optical forces. The next chapter goes into detail the penalty and benefit in micro ring resonator characterizations, which the most important nonlinearities in optical communication systems and optical trapping application.

CHAPTER 3

MICRORING RESONATOR SYSTEM FOR MEDICAL APPLICATIONS

In this chapter, we propose a design of device and system that can be used to generated the X-ray laser sources. The tiny system consists of a series of microring and nanoring resonators, whereas the powerful laser can be amplified to reach the very high power amplification. In principle, when a light pulse either soliton or Gaussian is input into the system, the nonlinear behavior is occurred, this is allowed the dramatically amplified. By controlling the ring parameters, the appropriate output power can be obtained, which can be modified to be suitable in either defense or medical applications.

3.1 Introduction

Recently, a scientist [39] has pointed out that it is time for the generation of the science fiction weapon known as a death ray being a realistic tool. It can be used for many applications, for instance, nuclear weapon or missile defense, laser gun and medical tools. In this work, we have shown the interesting results that can be fulfilled the required target by using a common laser within a tiny device. Since, an optical soliton is recognized as the powerful light source for high power laser. However, the pumping system is required before the soliton being generated. For simplicity, a Gaussian soliton is recommended to form the soliton instead of the pumping soliton. Moreover, one interesting aspect of the Gaussian soliton is that the non-dispersive soliton can be realized by using the 1.30 μm light source, which can be obtained by using the Gaussian soliton. Therefore, the use of a Gaussian soliton becomes a very attractive tool in the area of soliton investigation, whereas the simple system arrangement can be used to form the soliton behaviour within the medium for various investigations. Many research works have reported in use of a Gaussian pulse in both theoretical and experimental works [39-44]. Recently, the interesting aspect of light pulse propagating within a nonlinear microring device has been reported [45], where the transfer function of the output at resonant condition is derived and studied. They found that the broad spectrum of light pulse can be transformed to the discrete pulses. An optical soliton is recognized as a powerful laser pulse, which can be used to enlarge the optical bandwidth when

propagating within the nonlinear microring resonator [46, 47]. Moreover, the superposition of self-phase modulation (SPM) soliton pulses, where either bright or dark [48] solitons can generate the large output power. For further reading, many earlier works of soliton applications in either theory or experimental works are found in a soliton application book by Hasegawa et al [49]. Many of the soliton related concepts in fiber optic are discussed by Agrawal [50]. The problems of soliton-soliton interactions [51], collision [52], rectification [53] and dispersion management [54] are required to solve and address. In this work we are looking for a common laser source that can be used to generate the broad spectrum of lasers, especially, with the X-ray center wavelength. By using the suitable microring parameters, most of the results have shown that the optical signals, i.e. Gaussian pulse, can be amplified within the nonlinear ring resonator system, which is suitable for various applications such as medical tools, laser gun, laser sword and kitchen tools.

3.2 X-ray Laser Generation

Light from a monochromatic light source is launched into a ring resonator with constant light field amplitude (E_0) and random phase modulation, which is the combination of terms in attenuation (α) and phase(ϕ_0) constants, which results in temporal coherence degradation. Hence, the time dependent input light field (E_{in}), without pumping term, can be expressed as

$$E_{in}(t) = E_0 \exp^{-\alpha L + j\phi_0(t)} \tag{3.1}$$

where L is a propagation distance(waveguide length).We assume that the nonlinearity of the optical ring resonator is of the Kerr-type, i.e., the refractive index is given by

$$n = n_0 + n_2 I = n_0 + (\frac{n_2}{A_{eff}})P \tag{3.2}$$

where n_0 and n_2 are the linear and nonlinear refractive indexes, respectively. I and P are the optical intensity and optical power, respectively. The effective mode core area of the device is given by A_{eff}. For the microring and nanoring resonators, the effective mode core areas range from 0.10 to 0.50 μm [40, 55].

When a Gaussian pulse is input and propagated within a fiber ring resonator, the resonant output is formed, thus, the normalized output of the light field is the ratio between the output and input fields ($E_{out}(t)$ and $E_{in}(t)$) in each roundtrip, which can be expressed as [44, 45]

$$\left|\frac{E_{out}(t)}{E_{in}(t)}\right|^2 = (1-\gamma)\left[1-\frac{(1-(1-\gamma)x^2)\kappa}{(1-x\sqrt{1-\gamma}\sqrt{1-\kappa})^2+4x\sqrt{1-\gamma}\sqrt{1-\kappa}\sin^2(\frac{\phi}{2})}\right] \tag{3.3}$$

Equation (3.3) indicates that a ring resonator in the particular case is very similar to a Fabry-Perot cavity, which has an input and output mirror with a field reflectivity, (1- κ), and a fully reflecting mirror. κ is the coupling coefficient, and $x = \exp(-\alpha L/2)$ represents a roundtrip loss coefficient, $\phi_0 = kLn_0$ and $\phi_{NL} = kL(\frac{n_2}{A_{eff}})P$ are the linear and nonlinear phase shifts, $k = 2\pi/\lambda$ is the wave propagation number in a vacuum. Where L and α are a waveguide length and linear absorption coefficient, respectively. In this work, the iterative method is introduced to obtain the results as shown in equation (3.3), similarly, when the output field is connected and input into the other ring resonators. The input optical field as shown in equation (3.1), i.e. a Gaussian pulse, is input into a nonlinear microring resonator. By using the appropriate parameters, the chaotic signal is obtained by using equation (3.3). To retrieve the signals from the chaotic noise, we propose to use the add/drop device with the appropriate parameters. This is given in details as followings. The optical outputs of a ring resonator add/drop filter can be given by the equations (3.4) and (3.5).

$$\left|\frac{E_t}{E_{in}}\right|^2 = \frac{(1-\kappa_1)-2\sqrt{1-\kappa_1}\cdot\sqrt{1-\kappa_2}e^{-\frac{\alpha}{2}L}\cos(k_nL)+(1-\kappa_2)e^{-\alpha L}}{1+(1-\kappa_1)(1-\kappa_2)e^{-\alpha L}-2\sqrt{1-\kappa_1}\cdot\sqrt{1-\kappa_2}e^{-\frac{\alpha}{2}L}\cos(k_nL)} \tag{3.4}$$

and

$$\left|\frac{E_d}{E_{in}}\right|^2 = \frac{\kappa_1\kappa_2 e^{-\frac{\alpha}{2}L}}{1+(1-\kappa_1)(1-\kappa_2)e^{-\alpha L}-2\sqrt{1-\kappa_1}\cdot\sqrt{1-\kappa_2}e^{-\frac{\alpha}{2}L}\cos(k_nL)} \tag{3.5}$$

where E_t and E_d represents the optical fields of the throughput and drop ports respectively. The transmitted output can be controlled and obtained by choosing the suitable coupling ratio of the ring resonator, which is well derived and described by reference [45]. Where $\beta = kn_{eff}$ represents the propagation constant, n_{eff} is the effective refractive index of the waveguide, and the

circumference of the ring is $L = 2\pi R$, here R is the radius of the ring. In the following, new parameters will be used for simplification, where $\phi = \beta L$ is the phase constant. The chaotic noise cancellation can be managed by using the specific parameters of the add/drop device, which the required signals at the specific wavelength band can be filtered and retrieved. κ_1 and κ_2 are coupling coefficient of add/drop filters, $k_n = 2\pi / \lambda$ is the wave propagation number for in a vacuum, and the waveguide (ring resonator) loss is α = 0.5 dBmm^{-1}. The fractional coupler intensity loss is γ = 0.1. In the case of add/drop device, the nonlinear refractive index is neglected. In practice, the maximum wavelength that can be confined within the optical waveguide has been increased by using the composite of materials known as meta-materials [56, 57] , which is shown that the wavelength closed to few mm can be confined within the waveguide. In operation, light pulse is sliced to be the discrete signal and amplified within the first ring, where more signal amplification can be obtained by using the smaller ring device (second ring) as shown in Fig. 3.1.

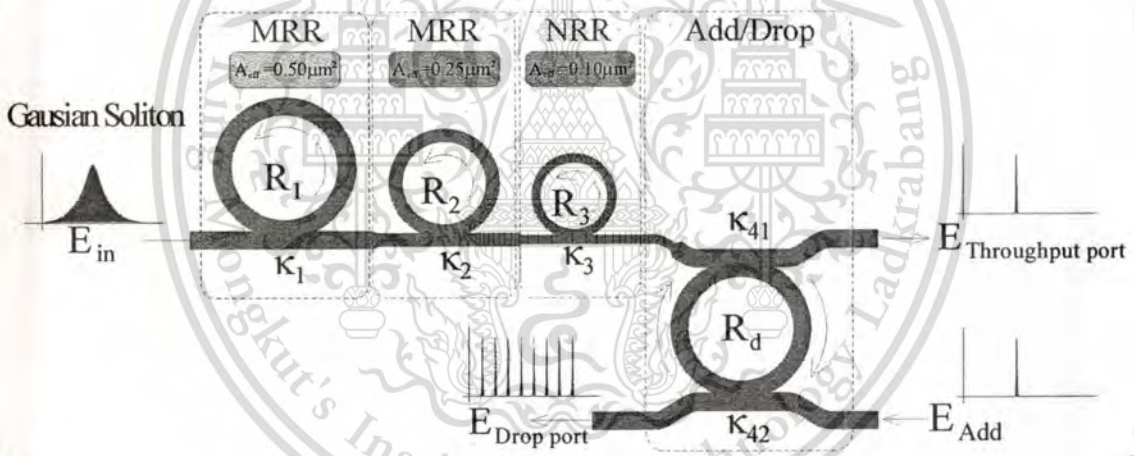

Figure 3.1 : A schematic of a Gaussian solution generation system for laser gun and laser tool, where R_s : ring radii, κ_s : coupling coefficients, R_d : an add/drop ring radius, $A_{eff\,s}$: effective areas

In Fig. 3.2 shows the simulation result of the continuous spectrum output when an optical pulse input into a micro ring resonator system, where the parameters used are $R_1 = 10\,\mu m$, $A_{eff\,1} = 0.50\,\mu m^2$, $R_2 = 7\,\mu m$, $A_{eff\,2} = 0.25\,\mu m^2$, $R_3 = 5\,\mu m$, $A_{eff\,3} = 0.10\,\mu m^2$, $\kappa_1 = 0.01$ and $\kappa_2 = \kappa_3 = 0.05$. Finally, the required signals can be obtained via a drop port of the add/drop filter. An optical field in the form of Gaussian pulse from a laser source at the specified center wavelength is input into the system.

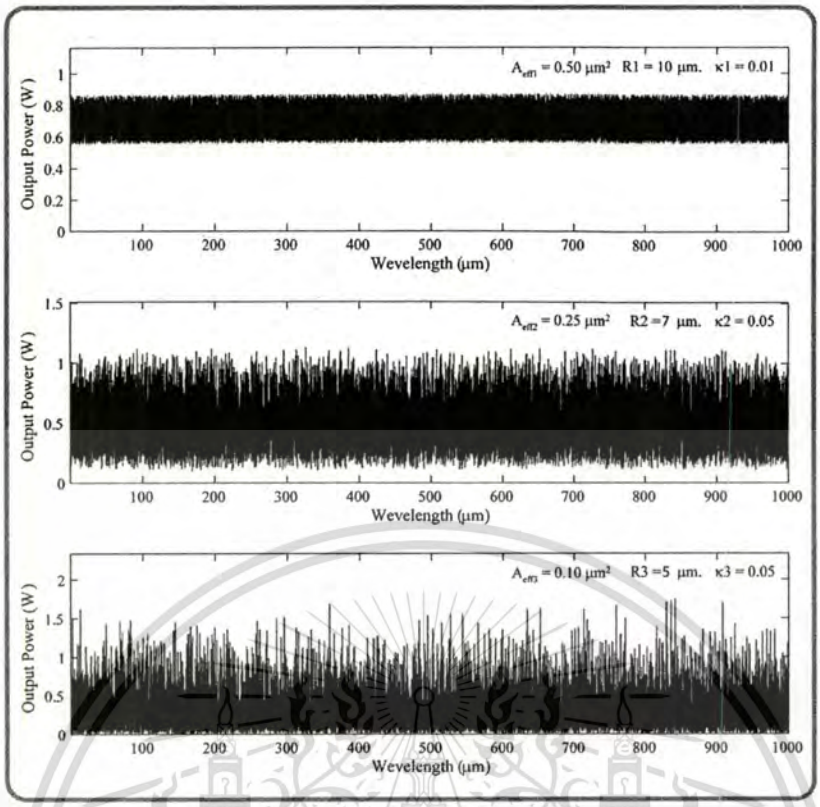

Figure 3.2 : The spectrum output when an optical pulse input into a micro ring resonator system

From Fig. 3.3, the Gaussian pulse with center wavelength (λ_0) at 3.0 mm, pulse width (Full Width at Half Maximum, **FWHM**) of 20 ns, peak power at 2 W is input into the system as shown in Fig. 3.3(a). The large bandwidth signals can be seen within the first microring device, and shown in Fig. 3.3(b). The suitable ring parameters are used, for instance, ring radii R_1= 15.0 μm, R_2= 9.0 μm, R_3= 5.0 μm, and R_d= 25.0 μm. In order to make the system associate with the practical device [55], the selected parameters of the system are fixed to n_0 = 3.34 (**InGaAsP/InP**), A_{eff} = 0.50 μm^2 and 0.25 μm^2 for a microring and add/drop ring resonator, respectively, α = 0.5 $dBmm^{-1}$, γ = 0.1. In this investigation, the coupling coefficient (kappa, κ) of the microring resonator is ranged from 0.10 to 0.96. The nonlinear refractive index of the microring used is n_2=2.2 x 10^{-17} m^2/W. In this case, the attenuation of light propagates within the system (i.e. wave guided) used is 0.5 $dBmm^{-1}$. After light is input into the system, the Gaussian pulse is chopped (sliced) into a smaller signal spreading over the spectrum due to the nonlinear effects [43], which is shown in Fig. 3.3(b). The large bandwidth signal is generated within the first ring device. In applications, the specific input or out wavelengths can be used and generated, where the suitable parameters are used and shown in the figures. In Fig. 3.4., the X-ray source with spectral width of 5 μm is obtained.

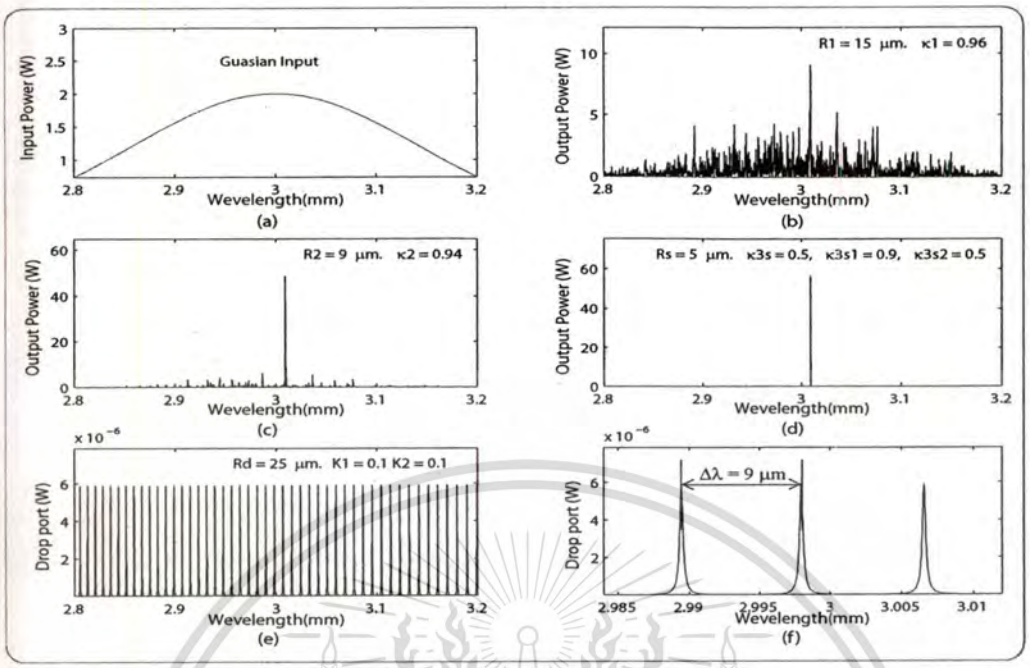

Figure 3.3 : Results of the X-ray laser pulses with center wavelength at 3 mm, where (a) the input Gaussian pulse, (b) the large bandwidth signals, (c) the filtering and amplifying signals, (d) the storage unit, (e) the drop port signals, (f) the X-ray sources, with spacing of 9 μm.

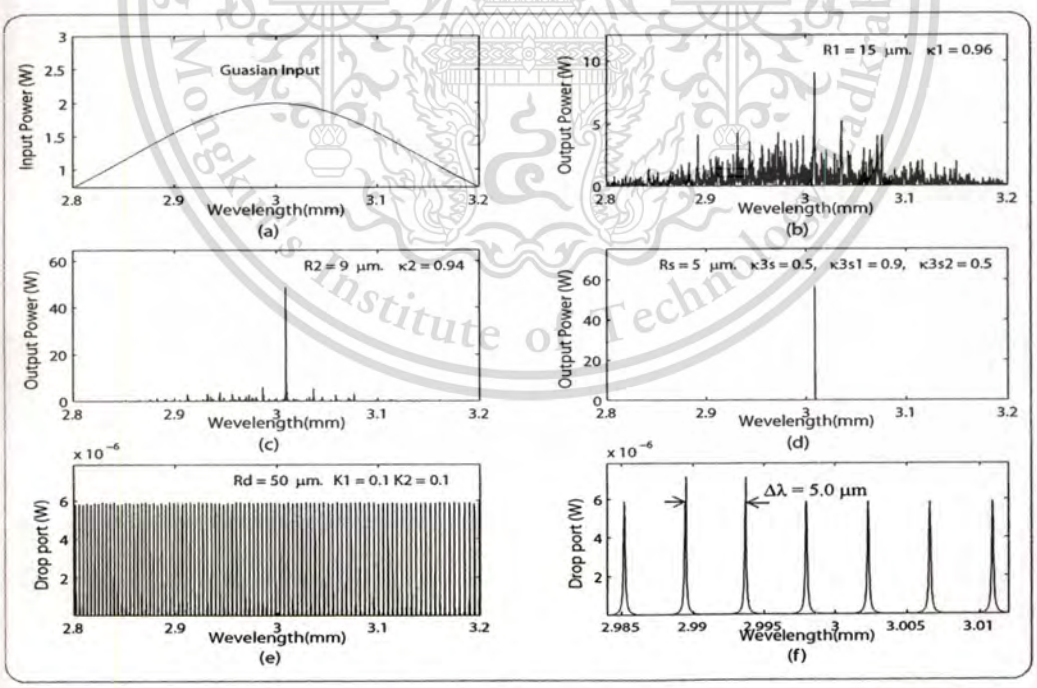

Figure 3.4 : Results of the X-ray laser pulses with center wavelength at 3 mm, where (a) the input Gaussian pulse, (b) the large bandwidth signals, (c) the filtering and amplifying signals, (d) the storage unit, (e) the drop port signals, (f) the X-ray sources, with spacing of 5 μm.

3.3 Laser Tool Mechanism

The results obtained have shown that the wide range of laser sources can be generated, while the generation of a high power light source can also be achieved. By using the obtained results from section 3.2, the laser tools system can be designed as shown in Fig. 3.5. In principle, for the safety reason, the controlled unit is very important in this design, therefore, each part of the system can be described as following details. After the input Gaussian pulse is amplified and reach the specified value, the optical energy can be storage within a ring resonator R_3 which has been designed and well described by reference [58]. The controlled parameters are the coupling coefficients, (κ_{31}, κ_3 and κ_{32}), that can be chosen to control the output energy. In applications, the certain number of light sources can be generated and stored within the embedded system, which can be available for the different requirements. For safety reason, the coupling coefficients $\kappa_{41}$and κ_{42} are designed to keep low output energy, where the increasing in energy can be obtained by controlling the optical switch. The absorber is operated when the switch is in the open status, where the small amount of output power is in the position. Furthermore, the semi-automatic running can be arranged by keeping the optical switch is in the operating position. Otherwise, it is the manual operation status as shown in Fig. 3.5.

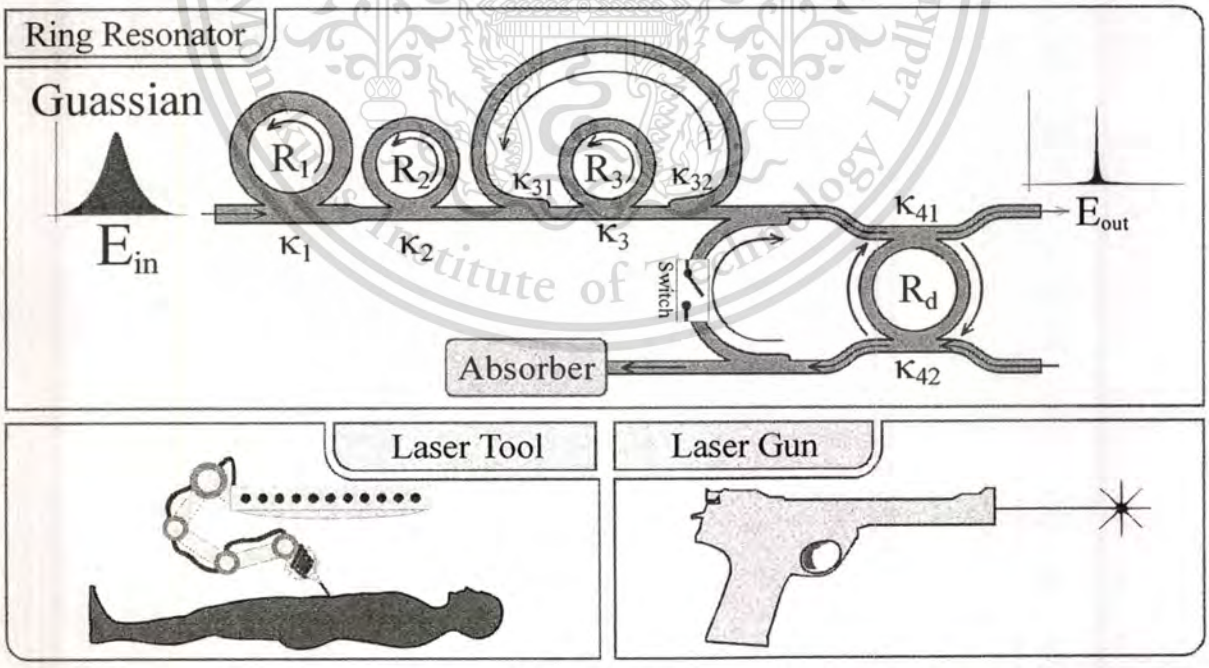

Fig. 3.5. Laser tool mechanism diagram, where R_s: ring radii, κ_s : coupling coefficients, R_d: an add/drop ring radius, A_{eff}s: Effective areas.

The various applications such as medical and kitchen tools, laser gun and laser sword can be operated by chosen the suitable laser center wavelength, output energy and bean size. However, the specific controlled by the scientific community is required.

3.4 Summary

This chapter, we have shown that the X-ray laser sources can be generated by using a Gaussian pulse propagating within the microring resonator system, which is available for medical tools with the wavelength center range from 3 mm. In applications, by using the wider range of ring parameters, the spectral range of the output can be covered wider range instead of fraction of nm. The large increasing in peak power is seen when light propagates from the large to small effective core area, where the other parameter is the coupling coefficient. Moreover, the center wavelength of the output lasers can also be designed to meet the different requirement, especially, for the medical surgery use. However, the amplified power is required to control to keep the device being the realistic tools.

CHAPTER 4

MULTITWEEZERS GENERATION AND CONTROL WITHIN A NANORING RESONATOR SYSTEM

In this chapter, we propose a system of dynamic potential well generation and control using light pulse control within an add/drop optical filter. The multiplexing signals of the dark solition with bright/Gaussian pulses are controlled, tuned, and amplified within the system. The optical storage rings are embedded within the add/drop optical filter system, whereas the generated optical signals can be stored and amplified within the design system. In application, the storage signals can be configured to be an optical trapping tool, which is known as an optical tweezer, where the high field peak or well can be formed. The advantages are that the dynamic well can be stored and the array of wells can be generated for multiple wells applications. The different in time of the first two dynamic wells of 1 ns is noted.

4.1 Introduction

A dark soliton exhibits an interesting and remarkable behavior when it is transmitted into an optical transmission system. It has the advantage of signal security when the ambiguity of signal detection becomes a problem of the cipher in the link. Recently, Sarapat et al [59]. have shown that the conversion of a dark soliton into a bright soliton can be realized using an add/drop filter. Here, the secured signals in the transmission are retrieved using a suitable add/drop filter that is connected to the transmission line. The other promising application of a dark soliton signal [60] is for the large guard band of two different frequencies, which can be achieved by using a dark soliton generation scheme. Furthermore, the dark soliton pulse shows a more stable behavior than the bright solitons with respect to perturbations, such as amplifier noise, fiber losses, and intra-pulse stimulated Raman scattering [61]. It is found that the dark soliton pulse propagation in a lossy fiber, spreads in time at approximately half the rate of bright solitons. One pays, however, for these advantages when generating dark soliton pulses. The other behavior is that dark soliton pulses are more difficult to detect than the bright soliton pulses [62]. Many earlier works of a dark soliton in fiber optics are found in Refs. [63-67]. Dark–bright soliton control has been investigated clearly by Sarapat et al., [59] where one of the advantages is that the dark soliton peak signal is always low level, which can be useful for secured signal communication in the transmission link. The other is formed when the high optical field is configured as an optical tweezer or

potential well, which is available for atom/molecule trapping. An optical tweezers technique has become a powerful tool for manipulation of micrometer-sized particles in three spatial dimensions [5]. Initially, the useful static tweezer was recognized and, now, the dynamic tweezer is realized in practical work. Typically, by using the continuous-wave lasers, the spatial control of atoms, beyond their trapping in stationary potentials, has been continuously gaining importance in the investigation of ultra cold gases and in the application of atomic ensembles and single atoms for cavity quantum electrodynamics and quantum information studies. Recent progress includes the trapping and control of single atoms in dynamic potentials, [68, 69] the submicron positioning of individual atoms with standing-wave potentials, [70, 71] micro-structured and dynamic traps for Bose–Einstein condensates [72-74] and, as another example, the realization of chaotic dynamics in atom-optics "billiards." [75-77] Recently, Mitatha et al.[78] have shown that the transfer of trapped atoms between two optical potentials could be performed. In this paper, we present a novel system of the optical tweezers storage using a dark-bright soliton pulse propagating within an add/drop optical filter. The multiplexing signals with different wavelengths of the dark solitions are controlled and amplified within the system. The dynamic behaviors of dark–bright soliton interaction are analyzed and described.

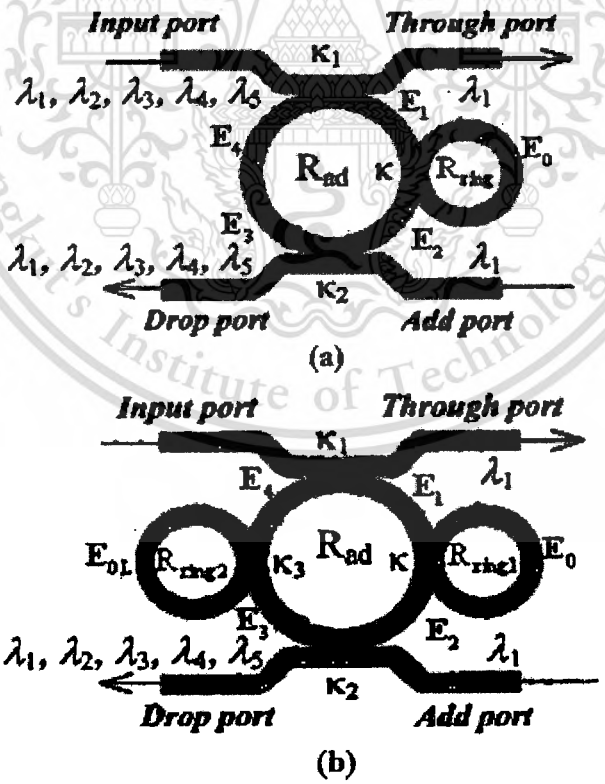

Figure 4.1: Schematic diagram of storage optical tweezers: (a) a single nanoring resonator and (b) two nanoring resonators.

The storage signals are controlled and tuned to be an optical probe, which is known as an optical tweezer. Optical tweezer storage is obtained by using the embedded nanoring resonators within the add/drop optical filter system. The controlled light pulses are added into the add port of the add/drop filter, for instance, bright soliton of Gaussian pulse. The different in time of the first two dynamic wells of 1 ns is noted by using the bright soliton input, while the potential well output stability is obtained by the Gaussian pulse input. In application, optical tweezers can be stored and trapped light/atom, which can form the dynamic tweezers and tweezers memory.

4.2 Principle and Method

We are looking for a stationary dark soliton pulse, which is introduced into the add/drop optical filter design, as shown in Fig. 4.1. The input optical field (E_{in}) of the dark soliton pulse input and the add optical field (E_{add}) of the bright soliton or Gaussian pulse at add port are given by [59, 60].

$$E_{in}(t) = A\tanh\left[\frac{T}{T_0}\right]\exp\left[\left(\frac{x}{2L_D}\right) - i\omega_0 t\right] \tag{4.1a}$$

$$E_{add}(t) = A\,\mathrm{sec}\,h\left[\frac{T}{T_0}\right]\exp\left[\left(\frac{x}{2L_D}\right) - i\omega_0 t\right] \tag{4.1b}$$

$$E_{add}(t) = E_0\exp\left[\frac{x}{2L_D} - i\omega_0 t\right] \tag{4.1c}$$

Where A and x are the optical field amplitude and propagation distance, respectively. T is a soliton pulse propagation time in a frame moving at the group velocity, T=t-$\beta_1^{\bullet} z$, where β_1 and β_2 are the coefficients of the linear and second-order terms of Taylor expansion of the propagation constant. L_D=$T_0^2/|\beta_2|$ is the dispersion length of the soliton pulse. T_0 is a soliton pulse propagation time at initial input (or soliton pulse width), where t is the soliton phase shift time, and the frequency shift of the soliton is ω_0. This solution describes a pulse that keeps its temporal width invariance as it propagates and thus is called a temporal soliton. When a soliton peak intensity ($|\beta_2/\Gamma T_0^2|$) is given, then T_0 is known. For the soliton pulse in the microring device, a balance should be achieved between the dispersion length (L_D) and the nonlinear length (L_{NL}=$1/\Gamma\phi_{NL}$), where Γ=$n_2^{\bullet} k_n$, is the length scale over which dispersive or nonlinear effects makes the beam become wider or narrower. For a soliton pulse, there is a balance between

dispersion and nonlinear lengths; hence, L_D=L_{NL}. For Gaussian pulse in Eq. (4.1c), E_0 is amplitude of optical field. When light propagates within the nonlinear material (medium), the refractive index (n) of light within the medium is given by

$$n = n_0 + n_2 I = n_0 + \frac{n_2}{A_{eff}} P \tag{4.2}$$

where n_0 and n_2 are the linear and nonlinear refractive indexes, respectively. I and P are the optical intensity and optical power, respectively. The effective mode core area of the device is given by A_{eff}. For the add/drop optical filter design, the effective mode core areas range from 0.50 to 0.10 μm^2, whereas the parameters were obtained by using the related practical material parameters (InGaAsP/InP) [79]. When a dark soliton pulse is input and propagated within a add/drop optical filter, as shown in Fig. 4.1, the resonant output is formed, and thus, the normalized output of the light field is the ratio between the output and input fields [$E_{out}(t)$ and $E_{in}(t)$] in each roundtrip, which is given by

$$\left|\frac{E_{out}(t)}{E_{in}(t)}\right|^2 = (1-\gamma)\left[1 - \frac{\left[1-(1-\gamma)x^2\right]\kappa}{(1-x\sqrt{(1-\gamma)\sqrt{1-\kappa}})^2 + 4x\sqrt{1-\gamma}\sqrt{1-\kappa}\sin^2(\phi/2)}\right]. \tag{4.3}$$

The closed form of Eq. (4.3) indicates that a ring resonator in this particular case is very similar to a Fabry–Perot cavity, which has an input and output mirror with a field reflectivity, (1-κ), and a fully reflecting mirror. κ is the coupling coefficient, and x=exp(-αL/2) represents a roundtrip loss coefficient, ϕ_0=$k_n L n_0$ and ϕ_{NL}=$k_n L n_2 |E_{in}|^2$ are the linear and nonlinear phase shifts, k_n=2π/λ is the wave propagation number in a vacuum, where L and α are waveguide length and linear absorption coefficient, respectively. In this work, the iterative method is introduced to obtain the results as shown in Eq. (4.3), and similarly, when the output field is connected and input into the other ring resonators. To retrieve the signals from the chaotic noise, we propose to use the add/drop device with the appropriate parameters. This is given in the following details. The optical circuits of ring-resonator add/drop filters for the through port and drop port can be given respectively,[59, 71] by

$$\left|\frac{E_t}{E_{in}}\right|^2 = \frac{(1-\kappa_1) - 2\sqrt{1-\kappa_1}\cdot\sqrt{1-\kappa_2}\,e^{-(\alpha/2)L}\cos(k_n L) + (1-\kappa_2)e^{-\alpha L}}{1+(1-\kappa_1)(1-\kappa_2)e^{-\alpha L} - 2\sqrt{1-\kappa_1}\cdot\sqrt{1-\kappa_2}\,e^{-(\alpha/2)L}\cos(k_n L)}, \tag{4.4}$$

$$\left|\frac{E_d}{E_{in}}\right|^2 = \frac{\kappa_1\kappa_2 e^{-(\alpha/2)L}}{1+(1-\kappa_1)(1-\kappa_2)e^{-\alpha L} - 2\sqrt{1-\kappa_1}\cdot\sqrt{1-\kappa_2}e^{-\alpha/2L}\cos(k_n L)}, \quad (4.5)$$

where E_t and E_d represent the optical fields of the through port and drop ports, respectively. $\beta=k_n n_{eff}$ is the propagation constant, n_{eff} is the effective refractive index of the waveguide, and the circumference of the ring is $L=2\pi R$, with R as the radius of the ring. In the following, new parameters will be used for simplification with $\phi=\beta L$ as the phase constant. The chaotic noise cancellation can be managed by using the specific parameters of the add/drop device, and the required signals can be retrieved by the specific users. κ_1 and κ_2 are the coupling coefficient of the add/drop filters, $k_n=2\pi/\lambda$ is the wave propagation number for in a vacuum, and where the waveguide (ring resonator) loss is α=0.5 dB mm^{-1}. The fractional coupler intensity loss is γ=0.1. In the case of the add/drop device, the nonlinear refractive index is neglected.

4.3 Dynamic Potential Well Generation

The schematic diagram of optical tweezer storage is designed and shown in Fig. 4.2. In operation, to form the memory unit, a nanoring resonator is embedded within the add/drop optical filter system. The nanoring resonator radius (R_{ring}) and the coupling coefficient (κ) are 100 nm and 0.15, respectively. The parameters of the add/drop optical filter system are set the same as in Section 4.2. In the system design, the dark soliton pulse is input into the input port through the coupler with the coupling coefficient is κ_1=0.35. It is partially input into the nanoring resonator with 20,000 roundtrips, where the storage signal is observed and the memory time is noted. The storage signals can be controlled by using the suitable parameters, especially, the coupling power (coupling coefficients) between the add/drop filter and nanoring resonator, which is given in Fig. 4.2. The output field (E_{t1}) at through port is expressed by

$$E_{t1} = AE_{i1} - BE_{i2}e^{-(\alpha L/2)-jk_n(L/2)} - \left[\frac{CE_{i1}(e^{-(\alpha L/2)-jk_n(L/2)})^2 + DE_{i2}(e^{-(\alpha L/2)-jk_n(L/2)})^3}{1-E(e^{-(\alpha L/2)-jk_n(L/2)})^2}\right], \quad (4.6)$$

when

$$A=\sqrt{(1-\gamma_1)(1-\gamma_2)},$$

$$B = \sqrt{1-\gamma_1(1-\gamma_2)\kappa_1(1-\kappa_2)}E_{0L},$$

$$C = \kappa_1(1-\gamma_1)\sqrt{(1-\gamma_2)\kappa_2}E_0E_{0L},$$

$$D = (1-\gamma_1)(1-\gamma_2)\sqrt{\kappa_1(1-\kappa_1)\kappa_2(1-\kappa_2)}E_0E_{0L}^2,$$

and

$$E = \sqrt{(1-\gamma_1)(1-\gamma_2)(1-\kappa_1)(1-\kappa_2)}E_0E_{0L}.$$

By electric fields, E_0 and E_{0L} are the field circulated within the nanoring at the right and left side of the add/drop optical filter. The power output (P_{t1}) at through port is

$$P_{t1} = |E_{t1}|^2 \tag{4.7}$$

The output field (E_{t2}) at drop port is

$$\begin{aligned} E_{t2} = {} & \sqrt{(1-\gamma_2)(1-\kappa_2)}E_{i2} \\ & - \left[\frac{\sqrt{(1-\gamma_1)(1-\gamma_2)\kappa_1\kappa_2}E_0E_{i1}e^{-(\alpha L/2)-jk_n(L/2)}}{1-\sqrt{(1-\gamma_1)(1-\gamma_2)(1-\kappa_1)(1-\kappa_2)}E_0E_{0L}(e^{-(\alpha L/2)-jk_n(L/2)})^2} \right] \\ & + \left[\frac{(1-\gamma_2)\sqrt{(1-\gamma_1)(1-\kappa_1)\kappa_2(1-\kappa_2)}E_0E_{0L}E_{i2}(e^{-(\alpha L/2)-jk_n(L/2)})^2}{1-\sqrt{(1-\gamma_1)(1-\gamma_2)(1-\kappa_1)(1-\kappa_2)}E_0E_{0L}(e^{-(\alpha L/2)-jk_n(L/2)})^2} \right] \end{aligned} \tag{4.8}$$

The power output (P_{t2}) at drop port is

$$P_{t2} = |E_{t2}|^2 \tag{4.9}$$

Simulation results of the dynamic optical tweezer signals within the light signal multiplexer are shown in Fig. 4.2. In this case, the bright soliton is input into the add port and the dynamic tweezers are shown in Figs. 4.2(a)–4.2(d). In Figs. 4.3(a)–4.3(f), the tweezers in the form of potential wells are seen. These tweezers can be used for atom/molecule trapping and transportation. The potential well depth (peak valley) can be controlled by adjusting the system parameters, for instance, the bright soliton input power at the add port and the coupling coefficients. The potential well of the tweezers is tuned to be the multiwells and seen at the add port, as shown in Fig. 4.3(f). In application, the optical tweezers in the

design system can be tuned and amplified as shown in Figs. 4.2 and 4.3. Therefore, the tunable optical tweezers can be controlled by the dark–bright soliton collision within the light signal multiplexer. This can be done by adjusting the parameters of the input power at the input and add ports, respectively.

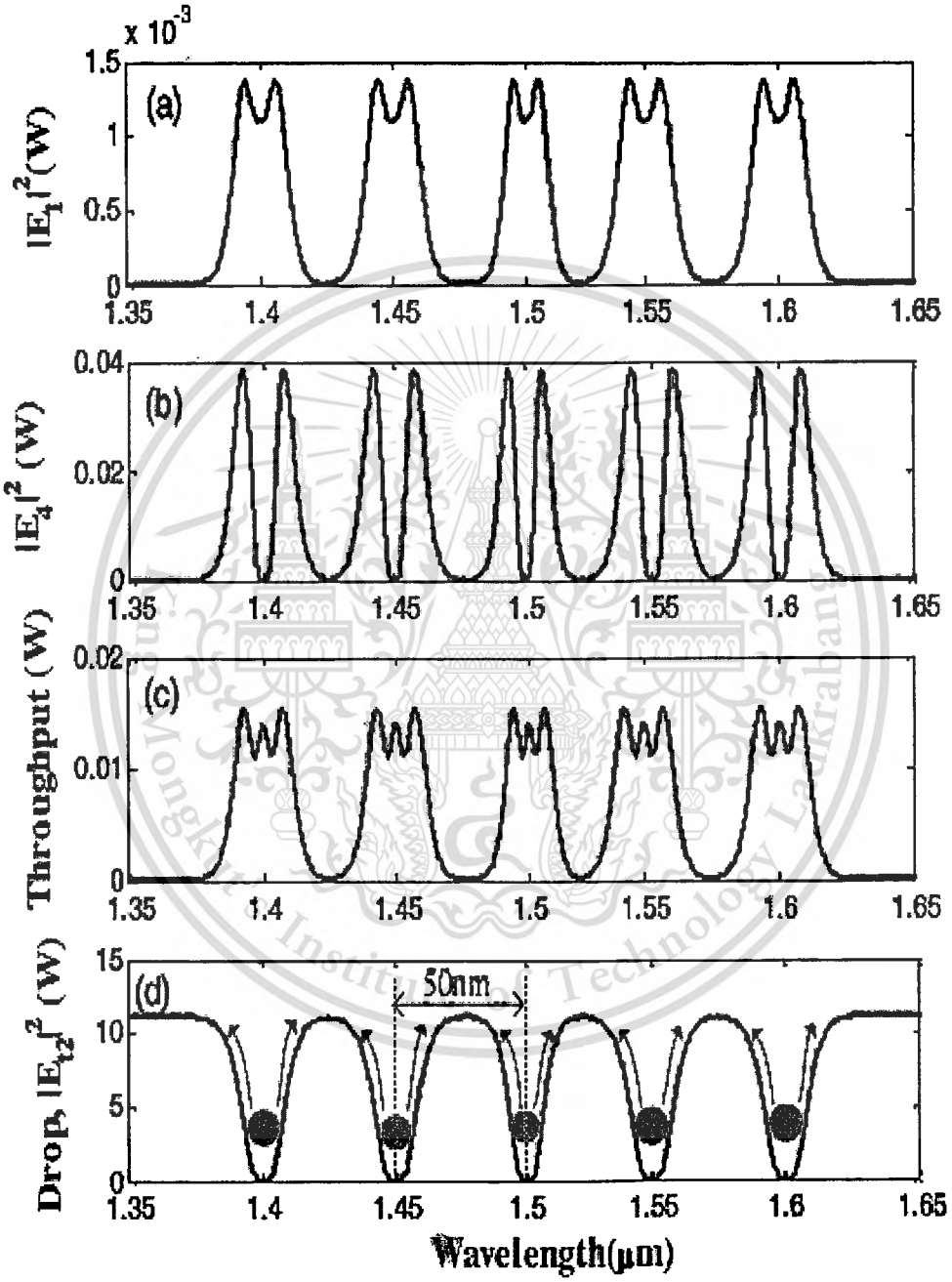

Figure 4.2: Simulation result of the dynamic tweezers with five different center wavelengths: (a) $|E_1|^2$, (b)$|E_4|^2$, and (c) are the through port and (d) drop port signals. The input signals are dark and bright soliton pulses at the input and control ports, respectively.

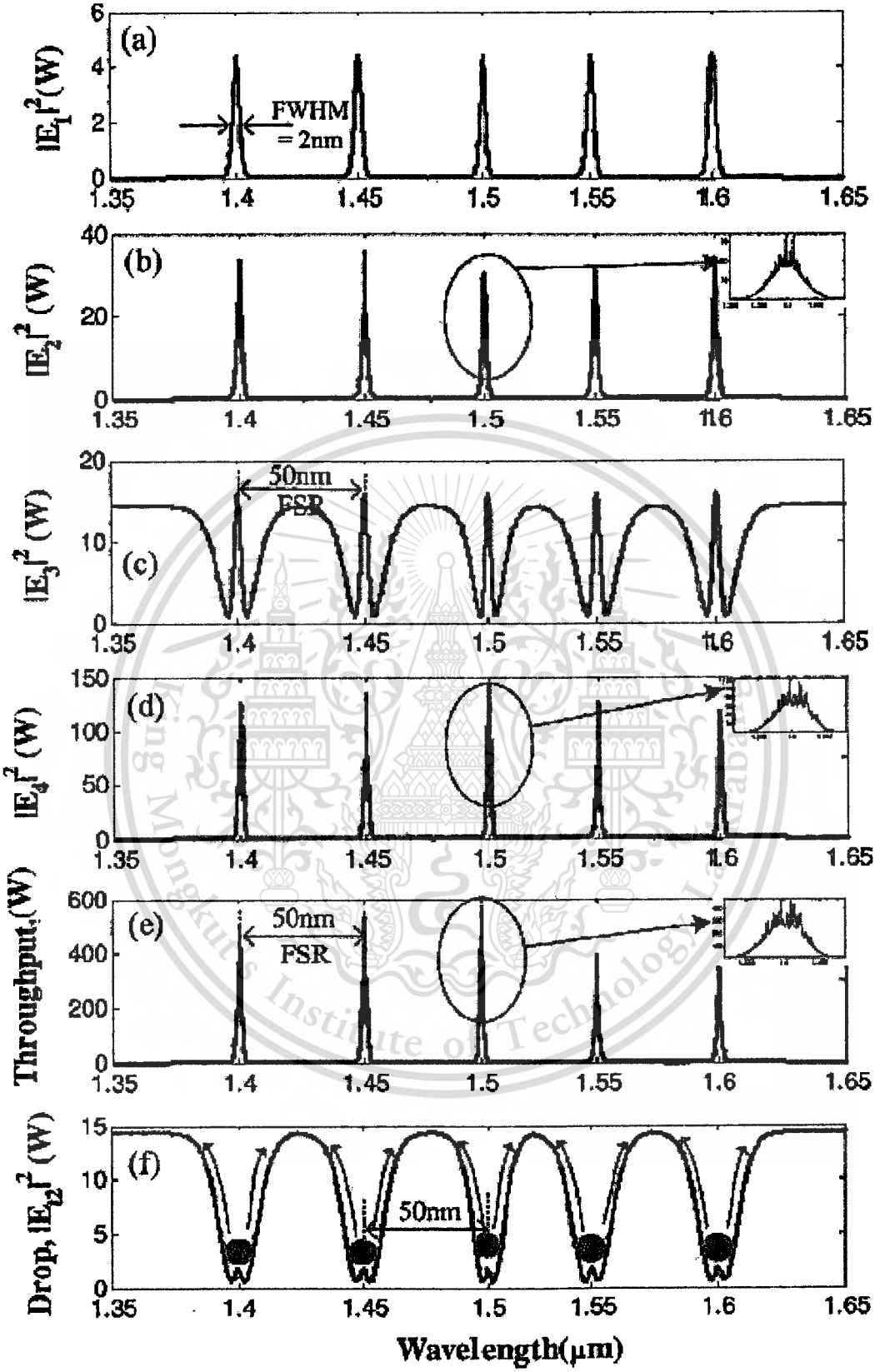

Figure 4.3: Simulation result of dynamic tweezers array with atoms for five different center wavelengths: (a) $|E_1|^2$, (b) $|E_2|^2$, (c) $|E_3|^2$, (d) $|E_4|^2$, (e) through port, and (f) drop port signals.

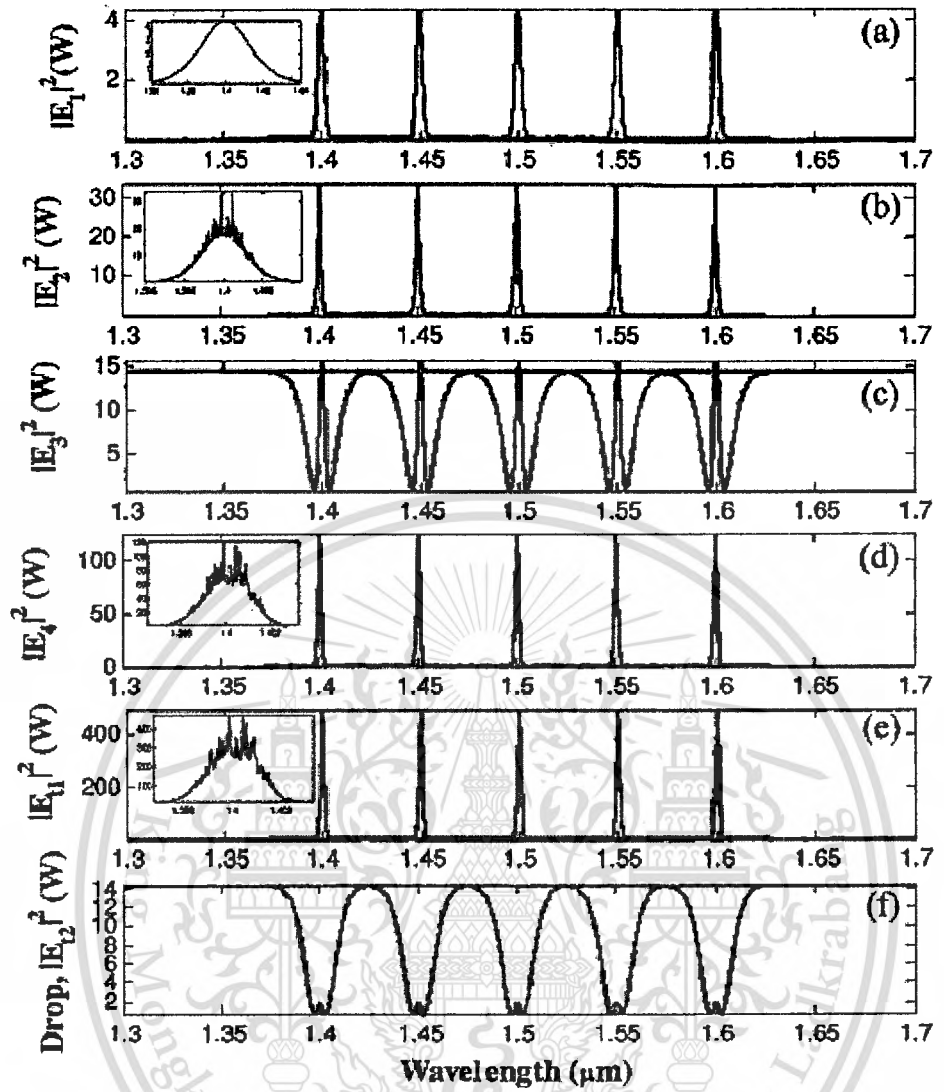

Figure 4.4: Simulation result of dynamic tweezers array with atoms for five different center wavelengths: (a) $|E_1|^2$, (b) $|E_2|^2$, (c) $|E_3|^2$, (d) $|E_4|^2$, (e) through port, and (f) drop port signals; the input signals are dark soliton and bright soliton pulses.

The output power at the through port is shown in Fig. 4.3(f). More results are as shown in Fig. 4.4. The potential well with the optical power of 15 W is observed. The coupling coefficients are given as κ_0=0.1, κ_1=0.35, κ_2=0.1, and κ_3=0.2, respectively. The ring radii are R_{ad}=1 μm, *R*ring1 =100 nm, and *R*ring2=100 nm. A_{eff} are 0.50, 0.25, and 0.25 μm^2 for the add/drop,[79] right and left ring resonators respectively.

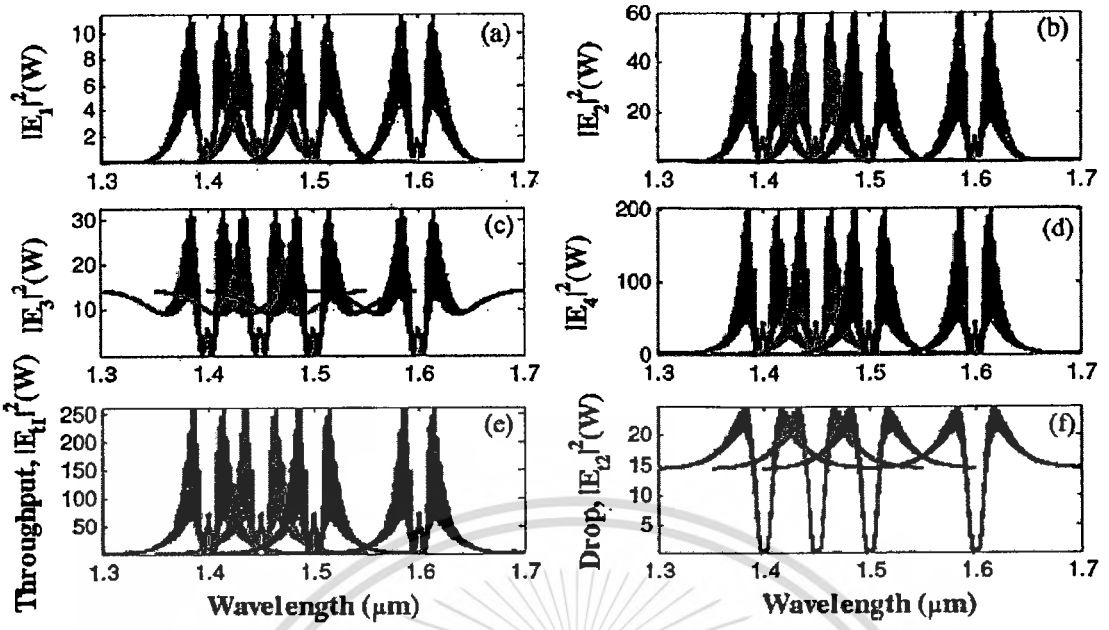

Figure 4.5: Results of the dynamic tweezers: (a) $|E_1|^2$, (b) $|E_2|^2$, (c) $|E_3|^2$, (d) $|E_4|^2$, (e) are the through port, and (f) drop port signals; the input signals are dark solitons and Gaussian pulses.

In Figs. 4.5(a)–4.5(f), we adjust the coupling coefficients, given as κ_0=0.2, κ_1=0.35, κ_2=0.1, and κ_3=0.1, respectively, the simulation results shown are (a) $|E_1|^2$, (b) $|E_2|^2$, (c) $|E_3|^2$, (d) $|E_4|^2$, (e) the through port, and (f) drop port signals. We found that the optical potential wells are stable, seen when the light pulse traveling in the add/drop design system, and the optical potential wells can be amplified and tunable as shown in Figs. 4.5(c), 4.5(d), and 4.5(e), whereas the multiwells are seen. For instance, the four potential wells are generated, whereas the well width of 16 nm with the peak power of 20 W is noted, as shown in Fig. 4.5(f). The signal free spectrum range of 50 nm is obtained, which becomes the trapping length limit of two adjacent optical tweezers in the system (optical multiplexer/ hybrid interferometer).

4.4 Conclusion

This chapter, we have shown that the dynamic tweezers can be used by using two nanoring resonators incorporating into the add/drop multiplexer. By using the reasonable dark–bright soliton input power, the dynamic optical tweezers can be controlled and stored. In this work, two types of optical tweezers can be configured by bright or dark soliton. In this case, the dynamic behavior can be controlled and used to form the hybrid devices. The numerical software used is the commercialized MATLAB-2008b, which is licensed by King Mongkut's Institute of Technology Ladkrabang, Thailand. In application, such a behavior can be used to confine the suitable size of light pulse or molecule, which

can be employed in the same way as the optical tweezers [80]. But in this case, the term dynamic probing has become the realistic function, where the trapped pulse or molecule within the period of time (memory) is plausible. Moreover, the multiple tweezers/wells storage configuration is allowed the storage array of tweezers/well, which is available for high density tweezer/well storage and high-capacity molecular transportation, which will be our continuous work.

CHAPTER 5

NANOSCOPIC VOLUME TRAPPING AND TRANSPORT USING A PANDA RING RESONATOR

In this chapter, we present a system of nanoscopic volume transmitter and receiver for drug delivery system using a PANDA ring resonator is proposed. By controlling some suitable parameters, the optical vortices (gradient optical fields/wells) can be generated and used to form the trapping tools in the same way as the optical tweezers. By using the intense optical vortices generated within the PANDA ring resonator, the nanoscopic volumes (drug) can be trapped and moved (transport) dynamically within the wavelength router or network. In principle, the trapping force is formed by the combination between the gradient field and scattering photons, which is reviewed. The advantage of the proposed system is that a transmitter and receiver can be formed within the same system (device), which is called a transceiver, which is available for nanoscopic volume (drug volume) trapping and transportation (delivery).

5.1 Introduction

Optical tweezers have been widely investigated in many research areas for such as in biology, physics, engineering, and nanotechnology, especially when the combination between nanomedicine and nanotechnology is formed, which is the interesting field. The use of nanotechnology in medicine for mesoscopic particle controlling and releasing has been reported by the authors in [81] and [82]. Obviously, the experiment of a single red blood cell (RBC) deformability test is performed by using the plastic optical trapping device in microfluidic chip, which was clearly experimentally demonstrated by Lee *et al.*[83], in which the optical trapping techniques was the firstly invented by Ashkin *et al.* [5]. Recently, the promising techniques of nanoscopic volume trapping and transportation within the add/drop multiplexer have been reported in both theory [84] and experiment [85], respectively, in which the transporter is known as an optical tweezer. Here, the optical tweezer generation technique has become a powerful tool for manipulation of nanometer-sized particles. To date, the useful static tweezers are well recognized and realized. Moreover, the use of dynamic tweezers is now also realized

in practical works [5, 86-87]. Schulz *et al.* [78] have shown that the transfer of trapped atoms between two optical potentials could be performed. In principle, an optical tweezers uses forces exerted by intensity gradients in the strongly focused beams of light to trap and move the nanoscopic volumes of matters, in which the other combination of force is induced by the interaction between photons, which is caused by the photon scattering effects. In application, the field intensity can be adjusted and tuned, in which the desired gradient field and scattering force can form the suitable trapping force. Hence, the appropriated force can be configured for the transmitter/receiver part, which can perform the long distance nanoscopic transportation. In this paper, the dynamic optical tweezers/vortices are generated using a dark soliton, bright soliton, and Gaussian pulse propagating within an add/drop optical multiplexer incorporating two nanoring resonators (PANDA ring resonator). The dynamic behaviors of soliton and Gaussian pulses are well described in [88]. By using the proposed system, the transceiver can be integrated and performed by using a single device. Here, the use of the transceiver to form the transportation of nanoscopic volumes of matters, especially for drug delivery, in the nanoscale regime can be realized.

5.2 Nanoscopic Volume Trapping Force Generation

In operation, the trapping forces are exerted by the intensity gradients in the strongly focused beams of light to trap and move the microscopic volumes of matters, in which the optical forces are customarily defined by the relationship [89]

$$F = \frac{Qn_m P}{c} \tag{5.1}$$

where Q is a dimensionless efficiency, n_m is the index of refraction of the suspending medium, c is the speed of light, and P is the incident laser power, measured at the specimen. Q represents the fraction of power utilized to exert force. For incident plane wave on a perfectly absorbing particle, Q is equal to 1. To achieve stable trapping, the radiation pressure must create a stable, three-dimensional equilibrium. Because biological specimens are usually contained in aqueous medium, the dependence of F on n_m can rarely be exploited to achieve higher trapping forces. Increasing the laser power is possible, but only over a limited range due to the possibility of optical damage. Q itself is therefore the main determinant of trapping force. It depends upon the numerical aperture (NA), laser wavelength, light polarization state, laser mode structure, relative index of refraction, and geometry of the particle.

Furthermore, in the Rayleigh regime, trapping forces decompose naturally into two components. Since, in this limit, the electromagnetic field is uniform across the dielectric, particles can be treated as induced point dipoles. The scattering force is given by [89]

$$F_{scatt} = n_m \frac{\langle S \rangle \sigma}{c}, \tag{5.2}$$

where

$$\sigma = \frac{8}{3}\pi (kr)^4 r^2 \left(\frac{m^2 - 1}{m^2 + 2} \right)^2 \tag{5.3}$$

Here σ is the scattering cross section of a Rayleigh sphere with radius $r \cdots \langle S \rangle$ is the time averaged Pointing vector, n is the index of refraction of the particle, $m = n / n_m$ is the relative index, and $k = 2\pi n_m / \lambda$ is the wave number of the light. The scattering force is proportional to the energy flux and points along the direction of propagation of the incident light. The gradient field (F_{grad}) is the Lorentz force acting on the dipole induced by the light field. It is given by [89]

$$F_{grad} = \frac{\alpha}{2} \nabla \langle E^2 \rangle \tag{5.4}$$

where

$$\alpha = n_m^2 r^3 \left(\frac{m^2 - 1}{m^2 + 2} \right) \tag{5.5}$$

Here α is the polarizability of the particle. The gradient force is proportional and parallel to the gradient in energy density (for m > 1). The large gradient force is formed by the large depth of the laser beam, in which the stable trapping requires that the gradient force in the $-\hat{z}$ direction, which is against the direction of incident light (dark soliton valley), and it is greater than the scattering force. By increasing the NA, when the focal spot size is decreased, the gradient strength is increased [89], which can be formed within the tiny system, for instance, a nanoscale device (nanoring resonator).

We are looking for the system that can generate the dynamic tweezers (optical vortices), in which the microscopic volume can be trapped and transmission via the communication link. Firstly, the stationary and strong pulse that can propagate within the dielectric material (waveguide) for the period of time required. Moreover, the gradient field is an important property required in this case. Therefore, a dark soliton is satisfied and recommended to perform those requirements. Secondly, we are looking for the device that optical tweezers can propagate and form the long distance link, in which the gradient

field (force) can be transmitted and received by using the same device. Here, the add/drop multiplexer in the form of a PANDA ring resonator which is well known and is introduced for this proposal, as shown in Figs. 5.1 and 5.2.

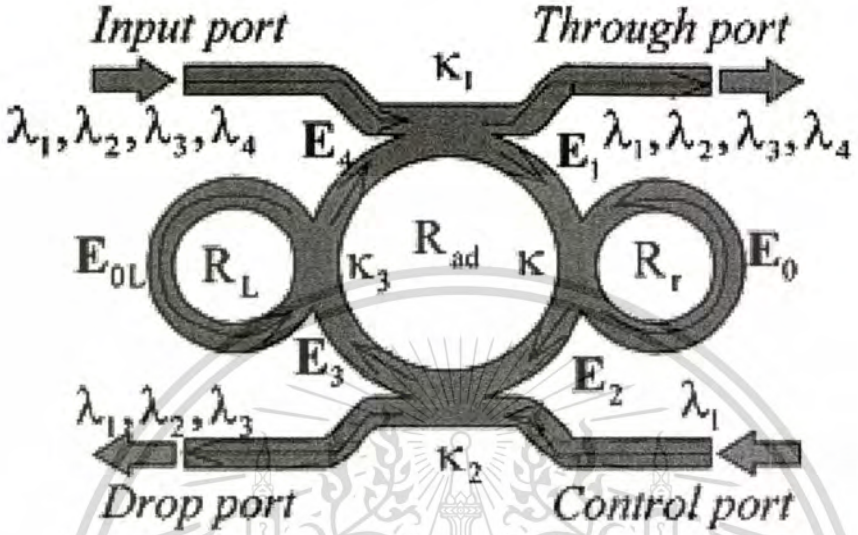

Figure 5.1: Schematic diagram of a proposed PANDA ring resonator.

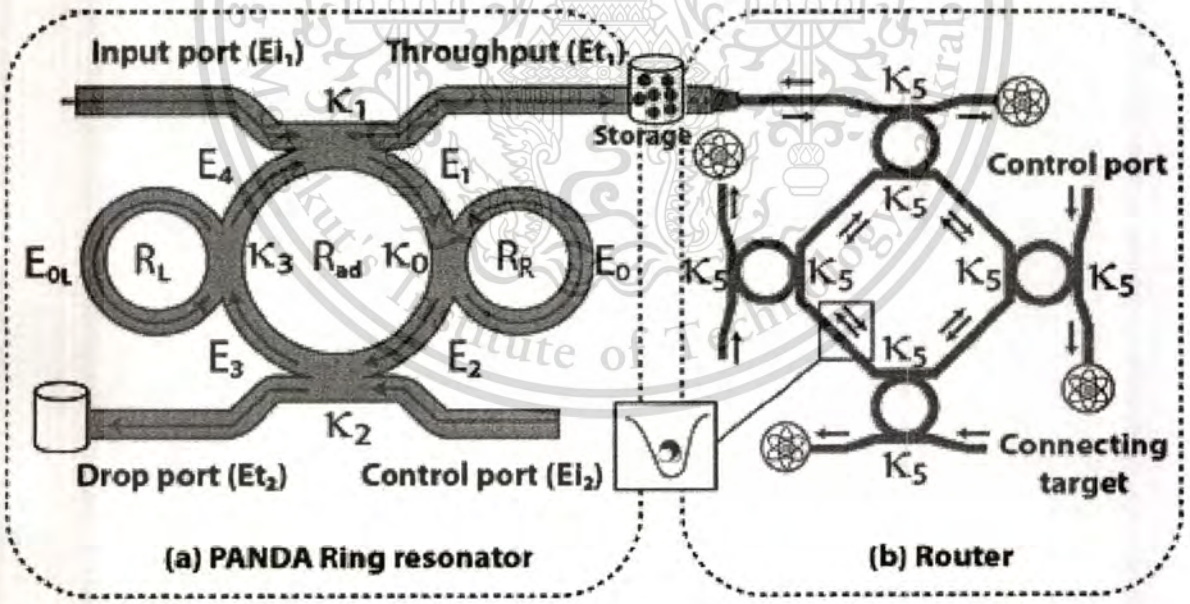

Figure 5.2: Schematic diagram of a drug delivery system using a transceiver and wavelength router, where (a) a PANDA ring resonator; (b) a wavelength router.

To form the multifunction operations, for instance, control, tune, amplify, the additional pulses are bright soliton and Gaussian pulse introduced into the system. The input optical field (E_{in}) and the add

port optical field (E_{add}) of the dark soliton, bright soliton and Gaussian pulses are given by [60], respectively

$$E_{in}(t) = A\sec h\left[\frac{T}{T_0}\right]\exp\left[\left(\frac{z}{2L_D}\right) - i\omega_0 t\right] \tag{5.6a}$$

$$E_{control}(t) = A\tanh\left[\frac{T}{T_0}\right]\exp\left[\left(\frac{z}{2L_D}\right) - i\omega_0 t\right] \tag{5.6b}$$

$$E_{control}(t) = E_0\exp\left[\left(\frac{z}{2L_D}\right) - i\omega_0 t\right] \tag{5.6c}$$

where A and z are the optical field amplitude and propagation distance, respectively. T is a soliton pulse propagation time in a frame moving at the group velocity, $T = t - \beta_1 z$, where β_1 and β_2 are the coefficients of the linear and second-order terms of Taylor expansion of the propagation constant. $L_D = T_0^2/|\beta_2|$ is the dispersion length of the soliton pulse. T_0 in the equation is a soliton pulse propagation time at initial input (or soliton pulse width), where t is the soliton phase shift time, and the frequency shift of the soliton is ω_0 This solution describes a pulse that keeps its temporal width invariance as it propagates, and thus is called a temporal soliton. When a soliton of peak intensity $(|\beta_2/\Gamma T_0^2|)$ is given, then T_0 is known. For the soliton pulse in the microring device, a balance should be achieved between the dispersion length (L_D) and the nonlinear length ($L_{NL} = 1/\Gamma\phi_{NL}$) Here $\Gamma = n_2 k_0$, is the length scale over which dispersive or nonlinear effects makes the beam become wider or narrower. For a soliton pulse, there is a balance between dispersion and nonlinear lengths. Hence $L_D = L_{NL}$ For a Gaussian pulse in (5.6c), E_0 is the amplitude of optical field. When light propagates within the nonlinear medium, the refractive index (n) of light within the medium is given by

$$n = n_0 + n_2 I = n_0 + (\frac{n_2}{A_{eff}})P \tag{5.7}$$

with n_0 and n_2 as the linear and nonlinear refractive indexes, respectively. I and P are the optical intensity and the power, respectively. The effective mode core area of the device is given by A_{eff} For the add/drop optical filter design, the effective mode core areas range from 0.10 to 0.50 μm^2, in which the parameters were obtained by using the related practical material parameters (InGaAsP/InP) [90].

When a dark soliton pulse is input and propagated within a add/drop optical filter as shown in Fig. 5.1, the resonant output is formed. Thus, the normalized output of the light field is defined as the ratio between the output and input fields [$E_{out}(t)$ and $E_{in}(t)$] in each roundtrip. This is given as Eq. 5.8 [45].

$$\left|\frac{E_{out}(t)}{E_{in}(t)}\right|^2 = (1-\gamma)\left[1-\frac{\left(1-(1-\gamma)x^2\right)\kappa}{\left(1-x\sqrt{1-\gamma}\sqrt{1-\kappa}\right)^2+4x\sqrt{1-\gamma}\sqrt{1-\kappa}\sin^2\left(\frac{\phi}{2}\right)}\right] \tag{5.8}$$

The close form of Eq. 5.8 indicates that a ring resonator in this particular case is very similar to a Fabry-Perot cavity. The input and output mirror with a field reflectivity are $(1-\kappa)$, and a fully reflecting mirror. κ is the coupling coefficient, and $x = \exp(-\alpha L/2)$ represents a roundtrip loss coefficient, $\phi_0 = kLn_0$ and $\phi_{NL} = kLn_2|E_{in}|^2$ are the linear and nonlinear phase shifts, $k = 2\pi/\lambda$ is the wave propagation number in a vacuum. L and α are the waveguide length and linear absorption coefficient, respectively. In this work, the iterative method is introduced to obtain the resonant results, and similarly, when the output field is connected and input into the other ring resonators.

In order to retrieve the required signals, we propose to use the add/drop device with the appropriate parameters. This is given in the following details. The optical circuits of ring resonator add/drop filters for the through port and drop port can be given by Eq. 5.9 and Eq. 5.10, respectively [44].

$$\left|\frac{E_t}{E_{in}}\right|^2 = \frac{\left[\left(1-\kappa_1\right)+\left(1-\kappa_2\right)e^{-\alpha L}-2\sqrt{1-\kappa_1}\cdot\sqrt{1-\kappa_2}e^{-\frac{\alpha}{2}L}\cos\left(k_nL\right)\right]}{\left[1+\left(1-\kappa_1\right)\left(1-\kappa_2\right)e^{-\alpha L}-2\sqrt{1-\kappa_1}\cdot\sqrt{1-\kappa_2}e^{-\frac{\alpha}{2}L}\cos\left(k_nL\right)\right]} \tag{5.9}$$

$$\left|\frac{E_d}{E_{in}}\right|^2 = \frac{\kappa_1\kappa_2 e^{-\frac{\alpha}{2}L}}{1+\left(1-\kappa_1\right)\left(1-\kappa_2\right)e^{-\alpha L}-2\sqrt{1-\kappa_1}\cdot\sqrt{1-\kappa_2}e^{-\frac{\alpha}{2}L}\cos\left(k_nL\right)} \tag{5.10}$$

Here E_t and E_d represent the optical fields of the through port and drop ports, respectively. $\beta = kn_{eff}$ is, the propagation constant, n_{eff} is the effective refractive index of the waveguide, and the circumference of the ring is $L = 2\pi R$, with R as the radius of the ring. The filtering signal can be managed by using the specific parameters of the add/drop device, and the required signals can be retrieved via the drop port output. κ_1 and κ_2 are the coupling coefficients of the add/drop filters,

$k_n = 2\pi/\lambda$ is the wave propagation number for in a vacuum, and the waveguide (ring resonator) loss is $\alpha = 0.5\,\mathrm{dBmm}^{-1}$. The fractional coupler intensity loss is $\gamma = 0.1$ In the case of the add/drop device, the nonlinear refractive index is not effect to the system, therefore, it is neglected. From Eq. 5.9, the output field (E_{t1}) at the through port is given by

$$E_{t1} = AE_{i1} - BE_{i2}e^{-\frac{\alpha L}{2} - jk_n\frac{L}{2}} - \left[\frac{CE_{i1}(e^{-\frac{\alpha L}{2} - jk_n\frac{L}{2}})^2 + DE_{i2}(e^{-\frac{\alpha L}{2} - jk_n\frac{L}{2}})^3}{1 - E(e^{-\frac{\alpha L}{2} - jk_n\frac{L}{2}})^2}\right] \tag{5.11}$$

when

$$A = \sqrt{(1-\gamma_1)(1-\gamma_2)},$$

$$B = \sqrt{1-\gamma_1(1-\gamma_2)\kappa_1(1-\kappa_2)}E_{0L},$$

$$C = \kappa_1(1-\gamma_1)\sqrt{(1-\gamma_2)\kappa_2}E_0E_{0L},$$

$$D = (1-\gamma_1)(1-\gamma_2)\sqrt{\kappa_1(1-\kappa_1)\kappa_2(1-\kappa_2)}E_0E_{0L}^2,$$

and

$$E = \sqrt{(1-\gamma_1)(1-\gamma_2)(1-\kappa_1)(1-\kappa_2)}E_0E_{0L}.$$

The electric fields E_0 and E_{0L} are the field circulated within the nanoring at the right and left side of add/drop optical filter. The power output (P_{t1}) at through port is written as

$$P_{t1} = |E_{t1}|^2 \tag{5.12}$$

The output field (E_{t2}) at drop port is expressed as

$$E_{t2} = \sqrt{(1-\gamma_2)(1-\kappa_2)}E_{i2} - \left[\frac{\sqrt{(1-\gamma_1)(1-\gamma_2)\kappa_1\kappa_2}E_0E_{i1}e^{-\frac{\alpha L}{2}-jk_n\frac{L}{2}} + XE_0E_{0L}E_{i2}\left(e^{-\frac{\alpha L}{2}-jk_n\frac{L}{2}}\right)^2}{1-YE_0E_{0L}\left(e^{-\frac{\alpha L}{2}-jk_n\frac{L}{2}}\right)^2}\right] \quad (5.13)$$

where

$$X = (1-\gamma_2)\sqrt{(1-\gamma_1)(1-\kappa_1)\kappa_2(1-\kappa_2)}$$

$$Y = \sqrt{(1-\gamma_1)(1-\gamma_2)(1-\kappa_1)(1-\kappa_2)}$$

The power output (P_{t2}) at drop port is

$$P_{t2} = |E_{t2}|^2 \quad (5.14)$$

5.3 Nanoscopic Volume Transport

The optical tweezers can be generated and trapped within the device and system as shown in Figs. 5.1 and 5.2. They can be used to transport and store the trapped volumes within the PANDA ring resonator and wavelength router, which can be used to form the nanoscopic volume transportation (drug delivery) via the waveguide [85]. The manipulation of trapped nanoscopic volumes within the optical tweezers is as shown in Fig. 5.3(f), where in this case study, the coupling coefficients are given as $\kappa_0 = 0.1$, $\kappa_1 = 0.35$, $\kappa_2 = 0.1$ and $\kappa_3 = 0.2$, respectively. The ring radii are $R_{add} = 1\mu m$ and $15\mu m$, $R_R = 100$ nm and $6\mu m$, $R_L = 100$ nm and $6\mu m$, respectively, in which the evidence of the practical device was reported by the authors in [91]. A_{eff} are 0.50, 0.25, and 0.25 μm^2: In this case, the dynamic tweezers (gradient fields) can be in the forms of bright soliton, Gaussian pulses, and dark soliton, which can be used to trap the required nanocopic volume.

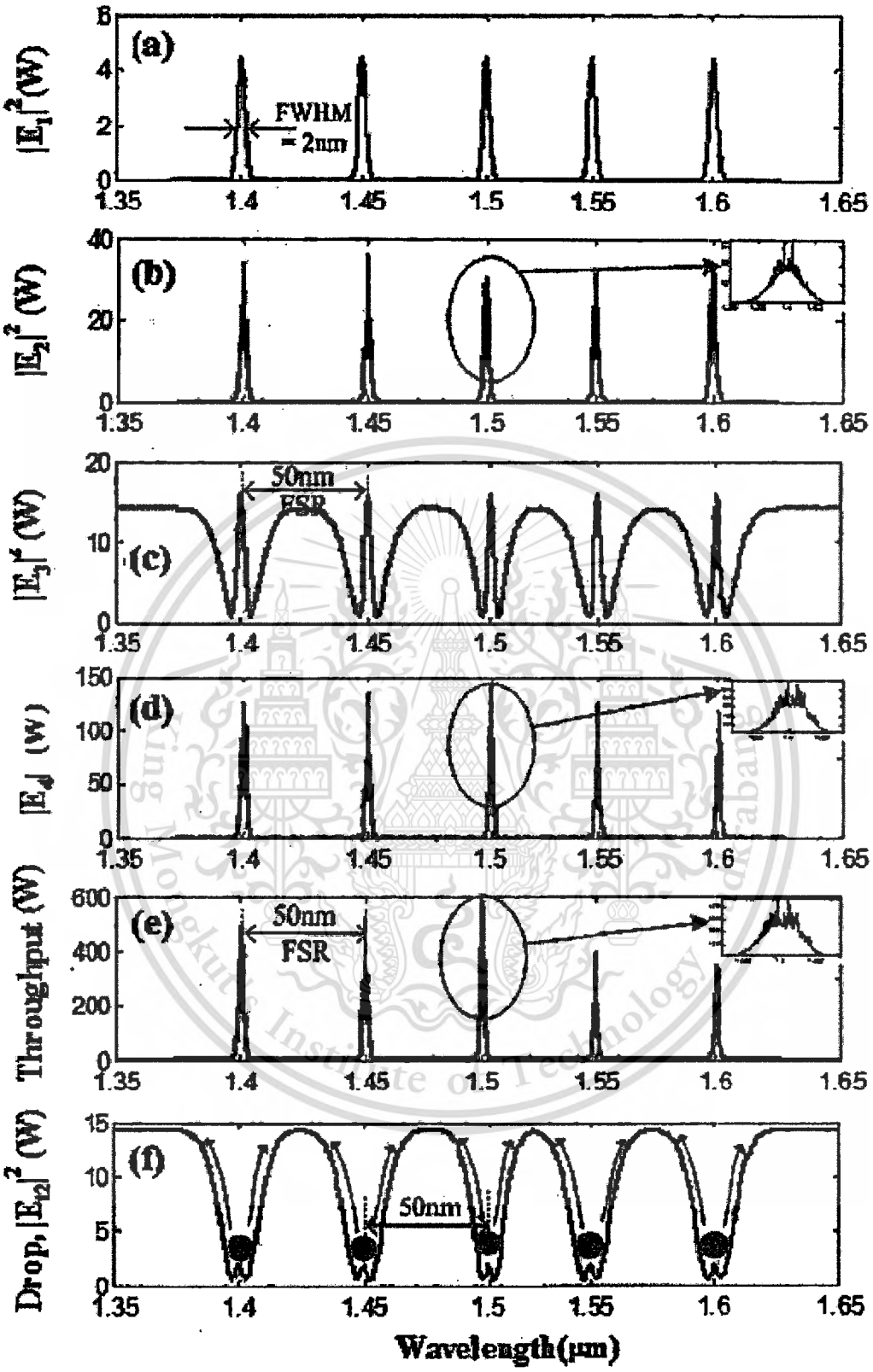

Figure.5.3: Results of the dynamic tweezers with nanoscopic volumes [Fig.5.2(f)], where the generated wavelengths are 1.4, 1.45, 1.5, 1.55, and 1.6 μm.

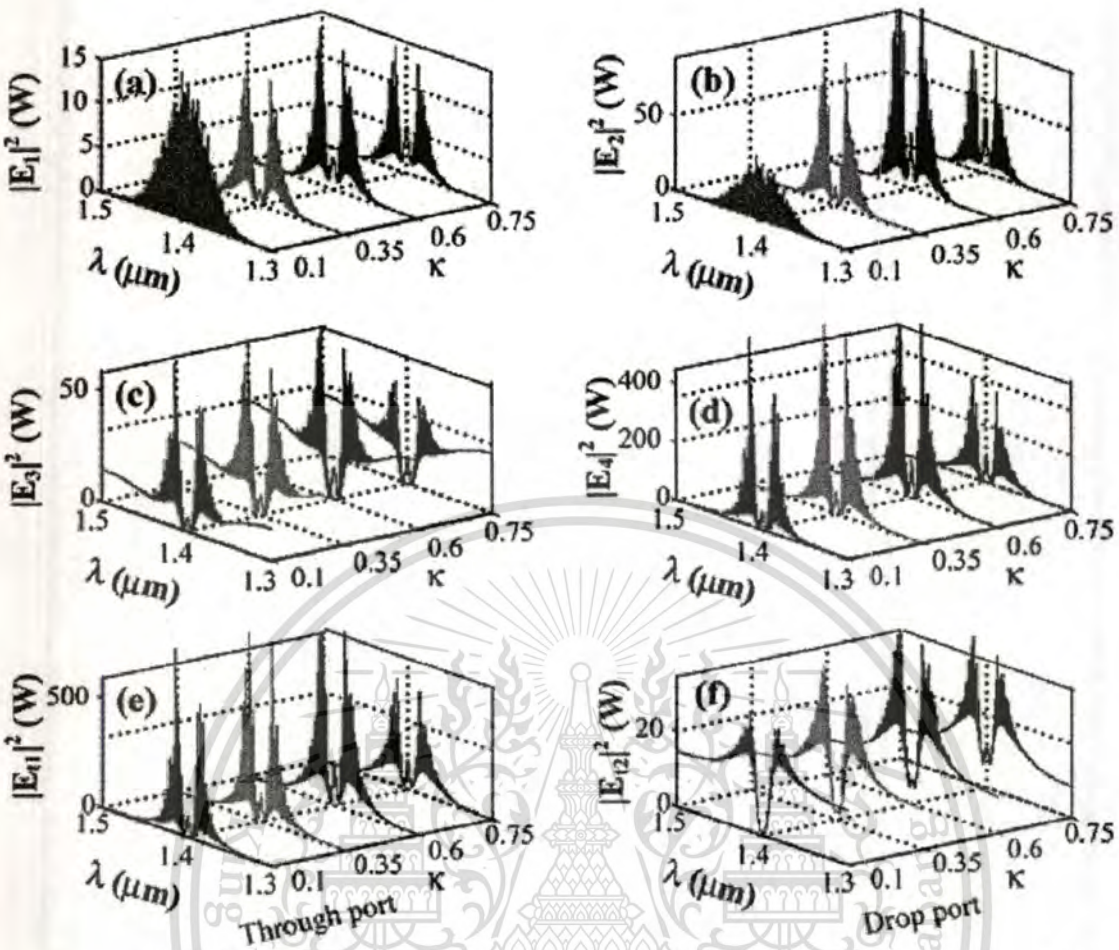

Figure.5.4: Simulation results of the tunable and amplified tweezers by varying the coupling coefficients.

In Fig. 5.4, there are five different center wavelengths of tweezers generated, where the dynamical movements are: (a) $|E_1|^2$, (b) $|E_2|^2$, (c) $|E_3|^2$, (d) $|E_4|^2$, e) through port; and f) drop port signals, where in this case all nanoscopic volumes are received by the drop port. The important aspect of the result is that the tunable tweezers can be obtained by tuning (controlling) the add (control) port input signal, in which the required number of nanoscopic volume (atom/photon/molecule) can be obtained and seen at the drop/through ports, otherwise, they propagate within a PANDA ring before collapsing/decaying into the waveguide. More results of the optical tweezers generated within the PANDA ring are as shown in Fig. 5.5, where in this case the bright soliton is used as the control port signal, and the output optical tweezers of the through and drop ports with different coupling constants are as shown in Fig. 5.5(e) and (f), respectively; the coupling coefficients are: 1) 0.1; 2) 0.35; 3) 0.6; and 4) 0.75.

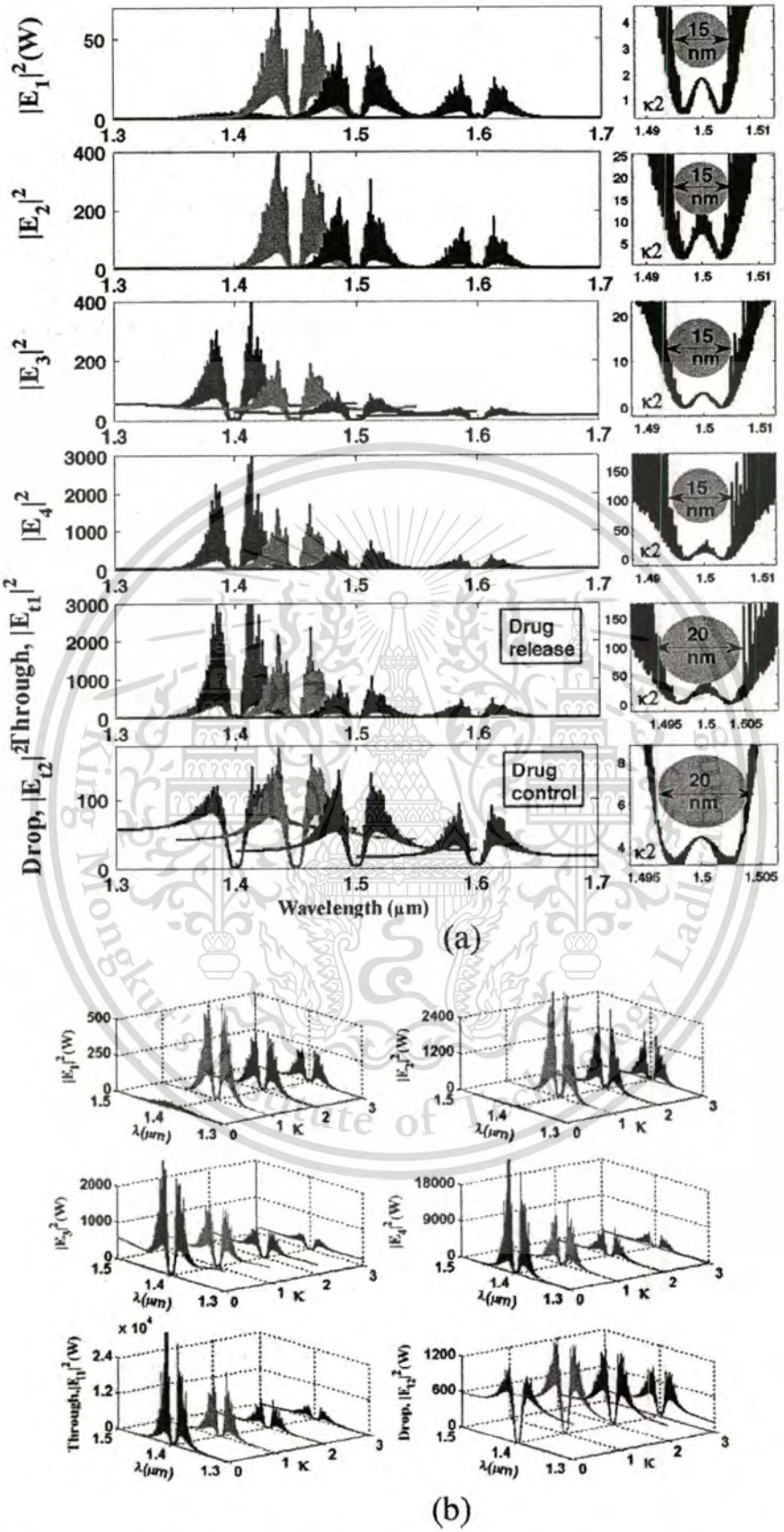

Figure.5.5:. Simulation results. (a) The controlling and releasing drug into drop and through put ports, respectively. (b) The tunable and amplified tweezers by varying the coupling coefficients.

In application, the trapped nanoscopic volumes can transport into the wavelength router via the through port, while the retrieved nanoscopic volumes are received via the drop port (connecting target), which can perform the drug delivery applications. The advantage of the proposed system is that the transmitter and receiver can be fabricated on-chip and alternatively operated by a single device in liquid core, which was the on-a chip design system, in which the use of light in waveguide that comprises a liquid core and a liquid cladding, which was reported by the authors in [92]. The nanoscopic effect on particle in liquid medium has been analyzed for the narrow systems, which was given by [93] and [94]. The system still effects in moving particles substantially smaller than the energizing wavelength, particularly, which is against the action of Brownian motion was given in [95]; however, the magnitude force can be varied and arranged by using the tunable tweezer amplitudes as shown in Fig. 5.5, where the tweezer widths of 20 and 20 nm can be obtained.

5.4 **Summary**

In this chapter, we have shown that the nanoscopic volumes can be trapped and transported into the optical waveguide by optical tweezers. By using a PANDA ring resonator and wavelength router, the long distance drug delivery can be transported and realized. By utilizing the reasonable dark soliton input power, the dynamic tweezers can be controlled and stored within the system, the obtained tweezers with free spectrum range (FSR) and the full width at half maximum (FWHM) of 50 and 2 nm are achieved, respectively; moreover, the tweezers amplification is also available by using nanoring resonators and modulated signals via the control port as shown in Figs. 5.4. and 5.5. In conclusion, we have also shown that the use of a transceiver to form the long distance nanoscopic volume transportation being realized by using the proposed system, in which the drug delivery can be performed via the wavelength router to the required (connecting) targets. However, the problems of large nanoscopic volume and neutral matter may cause a problem, in which the searching for new guide pipe and medium [96], for instance, nanotube and specific gas, will be the issue of investigation.

CHAPTER 6

CONCLUSION AND FUTURE WORK

6.1 General conclusion

The advancement of medical research in nano-scale have enabling us to understand the function of biological molecules at atomic level, which makes analysis and improved diagnostic accuracy and speed. That helps to the development of new tools and methods of treatment and more effective, such as highly sensitive sensors to detect biological molecules, transmission of drug molecules to target more accurately and in a reasonable amount. Or even to build artificial organs, which can mimic the function of various organs actually more closely. Research in light of significant progress and is light used in the development of research on the biological level, atoms, molecules that can be applied in the field of biotechnology in the confined particles in biological separations manipulation, making it possible. Uses of bio-optic systems have a wide throw which medical research has progressed steadily. It shows that the combination of nanoscale research in biological systems and optical systems. Which the research is develop a pace bowler in the field of research. In particular, research in molecular medicine.

. In the first part of this research has shown that the X-ray laser source has generated by using a Gaussian pulse input to the nano and micro ring resonator system. Makes it possible to generate output signals with the intensity of the light energy is high and a quarter wavelengths in the range of X-Ray and experimental results have demonstrated the possibility to be taken to design a device that can be used as official medical portable. Because, the system is compact and makes it convenient to use in a state of emergency and stay away from the hospital

In the second part of this work, an optical signal with a maximum power of the two peaks is very close and the signal resembles the potential energy wells. Which we refer to this as a signal that is generated called "Dynamic optical tweezers". This is a signal generated by the use of PANDA ring resonator. By using the reasonable dark-bright soliton input power, the dynamic optical tweezers can be control and stored. That can be used as a tool to confine the suitable size of light pulse or molecule within period of time is plausible. Moreover, the multiple tweezers/wells storage configuration is allowed the storage array of tweezers/wells storage and high-capacity molecular transportation.

In the third part is used the Dynamic optical tweezers to adjust the tuning of the distance from two the peak of power to a size appropriate to the size of the particles to be trapped and transported further. Using the ring resonator that is called PANDA ring redsonator. is a signal to the dark and bright soliton as a signal to the throughput port and add port (control port), respectively, the results show that the detention and transport of particles translucent. (molecular biology) is possible. However, it must also have research materials that are suitable to be used to study the flow of particles to the waveguide. Viscosity of the medium used to nourish the cells of living organisms.

6.2 Future Work

Optical tweezers are now widely used and they are particularly powerful in the field of microbiology to study cell–cell interactions, manipulate organelles without breaking the cell membrane and to measure adhesion forces between cells. In the next research we will describe a new concept of developing an optical tweezers source using a dark soliton pulse, which mean that the dynamic optical tweezers is plausible, therefore, the transportation of atoms/molecules in the optical network via a dark soliton being realized in the near future. In application, the trapped molecules/atoms by dynamic tweezers can be formed by using the tweezers array (multi tweezers), which is available for transportation in the routers [97], optical wireless link, artificial organ [98], diagnosis and treatment methods of diseases.

REFERENCES

[1] Ashkin, A. (1970), "Acceleration and Trapping of Particles by Radiation Pressure." Phys. Rev. Lett. 24(4): 156-159.

[2] Ashkin, A., J. M. Dziedzic and T. Yamane (1987), "Optical Trapping and Manipulation of Single Cells Using Infrared-Laser Beams." Nature 330(6150): 769-771.

[3] Ashkin, A. and Dziedzic, J.M. (1971), "Optical levitation by radiation pressure." Appl. Phys. Lett. 19: 283-285.

[4] Ashkin, A. and Dziedzic, J.M., "Observation of Radiation-Pressure Trapping of Particles by Alternating Light Beams." Phys. Rev. Lett. 54, 1245–1248 (1985)

[5] Ashkin, A., J. M. Dziedzic, J. E. Bjorkholm and S. Chu (1986). "Observation Of a Single-Beam Gradient Force Optical Trap For Dielectric Particles." Optics Letters 11(5): 288-290.

[6] E. Iannone, F. Matera, A. Mecozzi and M. Settembre, "Nonlinear optical communication networks," New York, pp. 35-36, 1998.

[7] N.V. Alekseeva, K.N. Alekseev, V.A. Balueva, G.P. Berman, A.K. Popov and V.Z. Yakhnin "Optical chaos in multiple degenerate four-wave mixing," Journal Optical and Quantum Electronics, Vol. 23, pp. 603-611, 1991.

[8] K.V. Peddanarappagari and M. Brandt-Pearce, "Volterra series transfer function of single-mode fibers," Journal of Light Wave Technology, Vol. 15, pp. 2232–2241, 1997.

[9] A. R. Chraplyvy, "Limitations on Light wave Communications Imposed by Optical-Fiber Nonlinearities," Journal of Lightwave Technology, Vol. 8, pp. 1548–1557, 1990.

[10] P.P. Yupapin, P. Saeung and W. Suwancharoen, "Coupler-loss and coupling-coefficient dependent of bistability and insatiability in fiber ring resonator: Nonlinear Behavior," Journal of Nonlinear Optical Physics & Materials. Vol. 16, pp. 111-118, 2007.

[11] J. Ohtsubo, "Chaos Synchronization and Chaotic Signal Masking in Semiconductor Lasers With Optical Feedback," IEEE J. of Quantum Electronics, Vol. 38, No. 9, pp.1141-1154, 2002.

[12] C. Juang,T.M. Hwang, J.Juang,and Wen-wei Lin. "A Synchronization Scheme using self-pulsating laser diode in optical chaotic communication," IEEE J. Quantum Electron, Vol. 36, pp. 300-304, 2000.

[13] K. Ikeda, H. Daido and O. Akimoto, "Optical turbulence: Chaotic behavior of transmitted light from a ring cavity", Phys. Rev. Lett. Vol. 45, pp. 709-712, 1980.

[14] P.P. Yupapin, P. Saeung and C. Li, "Characteristics of Complementary Ring-Resonator Add/Drop Filters Modeling by Using Graphical Approach", Elsevier, Journal Optics Communication, Vol. 272, pp. 81-86, 2007.

[15] B.E. Little and S.T. Chu. "Toward very large-scale integrated photonics", Opt. & Photon. News, vol. 11, 2000. pp. 24-29

[16] A. Hasegawa (Ed.), "New Trends in Optical Soliton Transmission Systems", AH Dordrecht, The Netherlands, Kluwer Academic Publishers, 1998

[17] G. P. Agrawal, "Fiber Optic Communication Systems", 3rd ed., Wiley, New York, 2002.

[18] G.P. Agrawal. "Nonlinear Fiber Optics", Academic Press, San Diego, CA, 2001

[19] A. Ashkin and J.M. Dziedzic. "Optical trapping and manipulation of viruses and bacteria", Science, 235:1517–1520, 1987.

[20] S. Chu, J.E. Bjorkholm, A. Ashkin, and A. Cable, "Experimental observation of optically trapped atoms", Phys. Rev. Lett, 57:314–317, 1986.

[21] D.M. Stamper-Kurn, M.R. Andrews, A.P. Chikkatur, S. Inouye, H.-J.Miesner, J. Stenger and W. Ketterle. "Optical confinement of a Bose-Einstein condensate", Phys. Rev. Lett., 80:2027–2030, 1998.

[22] E.R. Dufresne, G.C. Spalding, M.T. Dearing, S.A. Sheets, and D.G. Grier, "Computer-generated holographic optical tweezer arrays", Rev. Sci. Inst., 72:1810–1816, 2001.

[23] S.M. Block, D.F. Blair, and H.C. Berg. "Compliance of bacterial flagella measured with optical tweezers," Nature (London), 338:514–518, 1989.

[24] K. Svoboda, C.F. Schmidt, B.J. Schnapp, and S.M. Block. "Direct observation of kinesin stepping by optical trapping interferometry," Nature (London), 365:721–727, 1993.

[25] K. Svoboda and S.M. Block. "Optical trapping of metallic Rayleigh particles," Opt. Lett., 19:930–932, 1994.

[26] L.P. Ghislain, N.A. Switz, and W.W. Webb, "Measurement of small forces using an optical trap," Rev. Sci. Instr., 65:2762–2768, 1994.

[27] M.M. Burns, J.-M. Fournier, and J.A. Golovchenko. "Optical binding". Phys. Rev. Lett., 63:1233–1236, 1989.

[28] K. Visscher, G.J. Brakenhoff, and J.J. Krol. "Micromanipulation by multiple optical traps created by a single fast scanning trap integrated with the bilateral confocal scanning laser microscope," Cytometry, 14:105–114, 1993.

[29] M. Reicherter, T. Haist, E.U. Wagemann, and H.J. Tiziani. "Optical particle trapping with computer-generated holograms written on a liquid-crystal display," Opt. Lett., 24:608–610, 1999.

[30] J. Liesener, M. Reicherter, T. Haist, and H.J. Tiziani, "Multi-functional optical tweezers using computer-generated holograms," Opt. Commun., 185:77–82, 2000.

[31] J.E. Curtis, B.A. Koss, and D.G. Grier. "Dynamic holographic optical tweezers," Opt. Commun., 207:169–175, 2002.

[32] J. Leach, G. Sinclair, P. Jordan, J. Courtial, and M.J. Padgett. 3d, "Manipulation of particles into crystal structures using holographic optical tweezers," Opt. Expr., 12:220–226, 2004.

[33] V. Emiliani, D. Cojoc, E. Ferrari, V. Garbin, C. Durieux, M. Coppey-Moisan, and E. Di Fabrizio. "Wave front engineering for microscopy of living cells." Opt. Exp., 13:1395–1405, 2005.

[34] P.C. Mogensen and J. Gl¨uckstad. "Dynamic array generation and pattern formation for optical tweezers." Opt. Comm., 175:75–81, 2000.

[35] Malagnino N, Pesce G, Sasso A, Arimondo E, "Measurements of trapping efficieney and stiffness in optical tweezers." Optics Communications 2002; 214:15-24.

[36] Molloy JE, Padgett M: Light, "Action: optical tweezers." Contemporary Physics 2002; 43:241-258.

[37] Simpson NB, Allen L, Padgett MJ, "Optical tweezers and optical spanners with Laguerre-Gaussian modes." Journal of Modern Optics 1996; 43:2485-2491.

[38] Ishijima A, Doi T, Sakurada K, Yanagida T "Sub-piconewton force fluctuations of actomyosin in vitro." Nature 1991; 352: 301-306.

[39] J. Hecht, "Half a century of laser weapons," OPN, 20(2)(2009)14-21.

[40] D. Deng and Q. Guo, "Ince-Gaussian solitons in strongly nonlocal nonlinear media," Opt. Lett., 32(2007)3206-3208.

[41] G. Xia, Z. Wu, and J. Wu, "Effect of fiber chromatic dispersion on incident super-Gaussian pulse transmission in single-mode fibers," Chinese J. Phys., 41(2)(2003)118-120.

[42] S. Supparpola, Y. Sun and S. A. Chiramida, "Gaussian pulse decomposition: An intuitive model of electrocardiogram waveforms," Annals of Biomedical Engineering, 25(1997)252-260.

[43] P.K.A. Wai, K. Nakkeeran, "On the uniqueness of Gaussian ansatz parameters equations: generalized projection operator method," Phys. Lett., A, 332 (2004)239–243.

[44] P.P. Yupapin, P. Saeung and C. Li, "Characteristics of complementary ring-resonator add/drop filters modeling by using graphical approach," Opt. Commun., 272(2007)81-86.

[45] P.P. Yupapin and W. Suwancharoen, "Chaotic signal generation and cancellation using a microring resonator incorporating an optical add/drop multiplexer," Opt. Commun., vol. 280/2, pp. 343–350, 2007.

[46] P.P. Yupapin, N. Pornsuwanchroen and S. Chaiyasoonthorn "Attosecond pulse generation using nonlinear microring resonators," Microw. and Opt. Technol. Lett., 50(2008)3108-3111.

[47] N. Pornsuwancharoen and P.P. Yupapin "Generalized fast, slow, stop, and store light optically within a nanoring resonator," Microw. and Opt. Technol. Lett., 51(2009) 899-902.

[48] Y.S. Kivshar and B. Luther-Davies, "Dark optical solitons: Physics and applications," Phys. Rep., 298(1998)81-197.

[49] A. Hasegawa (Editor), "Massive WDM and TDM Soliton Transmission Systems," Kluwer Academic Publishers, Boston, 2000.

[50] G.P. Agrawal, "Nonlinear Fiber Optics," Academic Press, New York, 1995.

[51] Yu. A. Simonov and Tjon, "Soliton-soliton interaction in confining models," Phys. Lett., B 85(1979)380-384.

[52] J.K. Drohm, L.P. Kok, Yu. A. Simonov, J.A. Tjon and A.I. Veselov, "Collision and rotation of solitons in three space-time dimensions," Phys. Lett., B101(1981)204-208.

[53] T. Iizuka and Y.S. Kivshar, "Optical gap solitons in nonresonant quadratic media," Phys. Rev. E 59(1999)7148 - 7151.

[54] R. Ganapathy, K. Porsezian, A. Hasegawa, V.N. Serkin, "Soliton interaction under soliton dispersion management," IEEE Quantum Electron, 44(2008)383-390.

[55] Q. Xu and M. Lipson, "All-optical logic based on silicon micro-ring resonators," 15(3)(2007)924-929.

[56] M. Fujii, J. Leuthold and W. Freude, "Dispersion relation and loss of subwavelength confined mode of metal-dielectri-gap optical waveguides," IEEE Photon. Technol. Lett., 21(6)(2009)362-364.

[57] S. Mitatha and P.P. Yupapin, "Novel continuous spectrum generation system using a nano-waveguide for white light, short and sub-millimeter waves use," Microw. and Opt. Technol. Lett., 51(2009).

[58] P.P. Yupapin and N. Pornsuwancharoen, "Porposed nonlinear microring resonator arrangement for stopping and storing light," Photon. Technol. Lett., 21(6)(2009)404-406.

[59] K. Sarapat, N. Sangwara, K. Srinuanjan, P.P. Yupapin, and N. Pornsuwancharoen, "Novel dark-bright optical solitons conversion system and power amplification," Opt. Eng. 48(4), 045004 (2009).

[60] S. Mitatha, N. Pornsuwancharoen, and P.P. Yupapin, "A simultaneous short-wave and millimeter-wave generation using a soliton pulse within a nano-waveguide," IEEE Photonics Technol. Lett, vol 21, pp. 932–934 (2009).

[61] G.P. Agarwal, "Nonlinear Fiber Optics," 4th ed., Academic Press, New York (2007).

[62] C. Finot, J.M. Dudley, and G. Millot, "Generation of dark solitons by interaction between similaritons in Raman fiber amplifiers," Opt. Fiber Technol. 12, 217–226 (2006).

[63] S.F. Hanim, J. Ali, and P.P. Yupapin, "Dark soliton generation using dual Brillouin fiber laser in a fiber optic ring resonator," Microwave Opt. Technol. Lett. 52(4), 881–883 (2010).

[64] A.M. Weiner, J.P. Heritage, R.J. Hawkins, R.N. Thursten, E.M. Kirschner, D.E. Leaird, and W.J. Tomlinson, "Experimental observation of the fundamental dark soliton in optical fibers," Phys. Rev. Lett. 61(21), 2445–2448 (1988).

[65] T. Hong, Y.Z. Wang, and Y.S. Huo, "Temporal dark solitons in nonuniform Bose-Einstein condensates," Phys. Rev. A 58(4), 3128– 3133 (1997).

[66] S. Mitatha, "Dark soliton behaviors within the nonlinear micro and nanoring resonators and applications," Prog. Electromagn. Res. 99, 383–404 (2009).

[67] B.A. Malomed, A. Mostofi, and P.L. Chu, "Transformation of a dark soliton into a bright pulse," J. Opt. Soc. Am. B 17, 507–512 (2000).

[68] S. Bergamini, B. Darqui, M. Jones, L. Jacubowiez, A. Browaeys, and P. Grangier, "Holographic generation of micro trap arrays for single atoms by use of a programmable phase modulator," J. Opt. Soc. Am. B 21, 1889–1894 (2004).

[69] D.D. Yavuz, P.B. Kulatunga, E. Urban, T.A. Johnson, N. Proite, T. Henage, T.G. Walker, and M. Saffman, "Fast ground state manipulation of neutral atoms in microscopic optical traps," Phys. Rev. Lett. 96, 063001 (2006).

[70] D. Schrader, I. Dotsenko, M. Khudaverdyan, Y. Miroshnychenko, A. Rauschenbeutel, and D. Meschede, "Neutral atom quantum register," Phys. Rev. Lett. 93, 150501 (2004).

[71] J.A. Sauer, K.M. Fortier, M.S. Chang, C.D. Hamley, and M. S. Chapman, "Submicrometer position control of single trapped neutral atoms," Phys. Rev. A 69, 051804(R) (2004).

[72] T.P. Meyrath, F. Schreck, J.L. Hanssen, C.S. Chuu, and M.G. Raizen, "Bose-Einstein condensate in a box," Phys. Rev. A 71, 041604(R) (2005).

[73] V. Boyer, R.M. Godun, G. Smirne, D. Cassettari, C.M. Chandrashekar, A.B. Deb, Z.J. Laczik, and C.J. Foot, "Dynamic manipulation of Bose-Einstein condensates with a spatial light modulator," Phys. Rev. A 73, 031402(R) (2006).

[74] A.V. Carpentier, J. Belmonte-Beitia, H. Michinel, and V. M. Perez-Garcia, "Laser tweezers for atomic solitons," J. Mod. Opt. 55(17), 2819–2829 (2008).

[75] V. Milner, J.L. Hanssen, W.C. Campbell, and M.G. Raizen, "Optical billiards for atoms," Phys. Rev. Lett. 86, 1514–1516 (2001).

[76] N. Friedman, A. Kaplan, D. Carasso, and N. Davidson, "Observation of chaotic and regular dynamics in atom-optics billiards," Phys. Rev. Lett. 86, 1518–1520 (2001).

[77] M. Li and J. Arlt, "Trapping multiple particles in single optical tweezers," Opt. Commun. 281, 135–140 (2008).

[78] M. Schulz, H. Crepaz, F. Schmidt-Kaler, J. Eschner, and R. Blatt, "Transfer of trapped atoms between two optical tweezer potentials," J. Mod. Opt. 54(11), 1619–1626 (2007).

[79] Y. Kokubun, Y. Hatakeyama, M. Ogata, S. Suzuki, and N. Zaizen, "Fabrication technologies for vertically coupled microring resonator with multilevel crossing busline and ultracompact-ring radius," IEEE J. Sel. Top. Quantum Electron. 11, 4–10 (2005).

[80] T. Threepak, X. Luangvilay, S. Mitatha, and P.P. Yupapin, "Novel quantum-molecular transporter and networking via a wavelength router," Microwave Opt. Technol. Lett. 52(6), 1353–1357 (2010).

[81] G. Huang, J. Gao, Z. Hu, J. V. St. John, C. P. Bill, and D. Moro, "Controlled drug release from hydrogel nanoparticle networks," J. Controlled Release, vol. 94, pp. 303–311, 2004.

[82] S. Acharya and S. K. Sahoo, "PLGA nanoparticles containing various anticancer agents and tumour delivery by EPR effect," Adv. Drug Del. Rev., vol. 63, no. 3, pp. 170–183, Mar. 2011.

[83] W. G. Lee, K. Park, H. Bang, S. Chung, C. Chung, D. C. Han, and J. K. Chnag, "Single red blood cell deformability test using optical trapping in plastic microfluid chip," in Proc. 31st Annu. Int. IEEE EMBS, Special Topic Conf. Microtechnol. Med. Biol., May 2005, pp. 389–390.

[84] B. Piyatamrong, K.Kulsirirat, S. Mitatha, and P. P.Yupapin, "Dynamic potential well generation and control using double resonators incorporating in an add/drop filter," Mod. Phys. Lett. B, vol. 24, pp. 3071–3082, 2010.

[85] H. Cai and A. Poon, "Optical manipulation and transport of microparticle on silicon nitride microring resonator based add-drop devices," Opt. Lett., vol. 35, pp. 2855–2857, 2010.

[86] K. Egashira, A. Terasaki, and T. Kondow, "Photon trap spectroscopy applied to molecules adsorbed on a solid surface: Probing with a standing wave versus a propagating wave," App. Opt., vol. 80, pp. 5113–5115, 1998.

[87] A.V. Kachynski, A.N. Kuzmin, H.E. Pudavar, D.S. Kaputa, A.N. Cartwright, and P.N. Prasad, "Measurement of optical trapping forces by use of the two-photon-excited fluorescence of microspheres," Opt. Lett., vol. 28, pp. 2288–2290, 2003.

[88] M. Tasakorn, C. Teeka, R. Jomtarak, and P. P.Yupapin, "Multitweezers generation control within a nanoring resonator system," Opt. Eng., vol. 49, pp. 075002-1–075002-7, 2010.

[89] K. Svoboda and S. M. Block, "Biological applications of optical forces," Ann. Rev. Biophys. Biomol. Struct., vol. 23, pp. 247–282, 1994.

[90] Y. Kokubun, Y. Hatakeyama, M. Ogata, S. Suzuki, and N. Zaizen, "Fabrication technologies for vertically coupled microring resonator with multilevel crossing busline and ultracompact-ring radius," IEEE J. Sel. Topics Quantum Electron., vol. 11, pp. 4–10, 2005.

[91] J. Zhu, S.K. Ozdemir,Y. F. Xiao, L. Li, L. He, D.R. Chen, and L.Yang, "On-chip single nanoparticle detection and sizing by mode splitting in an ultrahigh-Q microresonator," Nature Photon., vol. 4, pp. 46–49, 2010.

[92] D.B. Wolfe, R.S. Conroy, P. Garsteck, B.T. Mayers, A. Michael, M.A. Fischbach, E. Kateri, K.E. Paul, M. Prentiss, and G.M. Whitesides, "Dynamic control of liquid-core

liquid-cladding optical waveguides," Proc. Natl. Acad. Sci., vol. 101, no. 34, pp. 2434–2438, 2004.

[93] L. Tongcang, S. Kheifets, D.M. Edellin, and M.G. Raizen, "Measurement of the instantaneous velocity of a Brownian particle," Science, vol. 328, no. 25, pp. 1673–1675, 2010.

[94] H.S. Chung and R. Hogg, "The effect of Brownian motion on particle size analysis by sedimentation," Powder Tech., vol. 41, pp. 211–216, 1985.

[95] P. Zemanek, A. Jonas, L. Sramek, and M. Liska, "Optical trapping of Rayleigh particles using a Gaussian standing wave," Opt. Commun., vol. 151, pp. 273–285, 1998.

[96] A. Ashkin, "Optical trapping and manipulation of neutral particles using lasers," in Proc. Natl. Acad. Sci., 1997, vol. 94, pp. 4853–4860.

[97] C. Vongchumyen, M. Tasakorn, S Mitatha and P.P. Yuppain, "An atom/molecule/DNA probing and transportation using dynamic optical tweezers via a wavelength router," Optik, vol 122, pp. 520-523, 2011.

[98] N. Suwanpayak, M.A. Jalil, M.S. Aziz, F.D. Ismail, J. Ali and P.P. Yuppain, "Blood cleaner on-chip design for artificial human kidney manipulation," International Journal of Nanomedicine, vol 6, pp. 957-964, 2011.

APPENDIX A

LIST OF PUBLICATIONS

Publication in 2011

1. M. A. Jalil, M. Tasakorn, N. Suwanpayak,. J. Ali, P. P. Yupapin, **Nanoscopic Volume Trapping and Transportation Using a PANDA Ring Resonator for Drug Delivery,** IEEE Transaction on NanoBioScience, Volume 10, No. 2, June 2011, Page(s): 106 - 112
2. C. Vongchumyen, M. Tasakorn, S. Mitatha, P.P. Yupapin, **An atom/molecule/DNA probing and transportation using dynamic optical tweezers via a wavelength router,** Optik International Journal for Light and Electron Optics, Volume 122, Issue 6, March 2011, Pages 520-523

Publication in 2010

1. M. Tasakorn, C. Teeka, R. Jomtarak and P.P. Yupapin, **Multi Tweezers Generation Control within a Nanoring Resonator System,** Optical Engineering, Volume 49, Issue 7, July 2010, Pages 075002 - 1-6.
2. N. Pornsuwancharoen, M. Tasakorn, S. Julajaturasirarath, K. Chaiyawong, P.P. Yupapin, **Multi-variable quantum tweezers generation using photon entanglement,** Nano Communication Networks, Volume 1, Issue 2, June 2010, Pages 131-137

Publication in 2009

1. Ura Dunmeekaew, Metha Tasakorn, Nithiroth Pornsuwancharoen, Preecha P. Yupapin, **New wavelength division multiplexing bands generated by using a Gaussian pulse in a microring resonator system,** Physics Procedia, Vol. 2(1), 2009, pp. 33-38.
2. Metha Tasakorn, Nithiroth Pornsuwancharoen, Wanchai Khunnam, and Preecha P. Yupapin, **High resolution multi-color imaging for bio-cell microscopy,** Physics Procedia, Vol. 2, 2009. (Article in press)

BIOGRAPHY

Name: **Mr. Metha Tasakorn**

Organization: Department of Electrical Engineering, Faculty of Industrial and Technology, Rajamamgala University of Technology Isan, Sakon Nakhon Campus, Thailand 47160.

E-mail : may_tsk@hotmail.com, mtasakorn@gmail.com

Educations:

Year	Degree	Major	Institution	Country
1995	B.Ind	Industrial Electrical Technology.	KMUTNB	Thailand
2002	M.S.	Electronique Electrotechnique and Automatique.	PARIS XII	France